

Constraining ultra slow roll inflation using cosmological datasets

H. V. Ragavendra^{1*}, Anjan Kumar Sarkar^{2†} and Shiv K. Sethi^{1‡}

¹Raman Research Institute, C. V. Raman Avenue, Sadashivanagar, Bengaluru 560080, India

²National Centre for Radio Astrophysics, TIFR, Pune University Campus, Post Bag 3, Pune 411 007, India.

E-mail: *ragavendra@rrimail.rrri.res.in, †asarkar@ncra.tifr.res.in, ‡sethi@rrri.res.in

Abstract. In recent years, the detection of gravitational waves by LIGO and PTA collaborations have raised the intriguing possibility of excess matter power at small scales. Such an increase can be achieved by ultra slow roll (USR) phase during inflationary epoch. We constrain excess power over small scales within the framework of such models using cosmological datasets, particularly of CMB anisotropies and Lyman- α . We parameterize the USR phase in terms of the e-fold at the onset of USR (counted from the end of inflation) \bar{N}_1 and the duration of USR phase ΔN . The former dictates the scale of enhancement in the primordial power spectrum, while the latter determines the amplitude of such an enhancement. From a joint dataset of CMB, SNIa and galaxy surveys, we obtain $\bar{N}_1 \lesssim 45$ with no bound on ΔN . This in turn implies that the scales over which the power spectrum can deviate significantly from the nearly scale invariant behavior of a typical slow-roll model is $k \gtrsim 1 \text{ Mpc}^{-1}$. On the other hand, the Lyman- α data is sensitive to baryonic power spectrum along the line of sight. We consider a semi-analytic theoretical method and high spectral-resolution Lyman- α data to constrain the model. The Lyman- α data limits both the USR parameters: $\bar{N}_1 \lesssim 41$ and $\Delta N \lesssim 0.4$. This constrains the amplitude of the power spectrum enhancement to be less than a factor of hundred over scales $1 \lesssim k/\text{Mpc}^{-1} \lesssim 100$, thereby considerably improving the constraint on power over these scales as compared to the bounds arrived at from CMB spectral distortion.

Contents

1	Introduction	1
2	Model of ultra-slow roll inflation	3
3	Results	6
3.1	CMB, SNIa and galaxy survey data	7
3.2	Lyman- α forest	11
4	Conclusion	14
A	Choice of parameters determining spectra over large scales	17

1 Introduction

The current cosmological data bears out the Λ CDM model at large scales ($k \gtrsim 0.2 \text{ Mpc}^{-1}$). At smaller scales, the situation remains unsettled. While a set of observables suggest decrement of matter power at small scales, the enhancement of primordial scalar power at small scales is also a feature that has been sought after in the recent literature. Such enhancement leads to production of primordial black holes (PBHs) and secondary gravitational waves (GWs) and so models of primordial universe that effect such a feature have been constructed and examined extensively (see for reviews, Refs. [1–3]). This effort has been spurred by the detection of mergers of supermassive black-holes by LIGO and, recently, with the data release of PTA which claims the detection of stochastic GWs [4–8]. It has been suggested that the supermassive black-holes of the LIGO merger events are primordial black holes (see Refs. [9–14] and references therein). The data of PTA suggests that the scalar-induced secondary GWs seem to be the best-fit candidate to explain the signal [15–24].

Amongst the many models of early universe that may lead to the desired enhancement of scalar power over small scales, inflationary models with a brief epoch of ultra slow roll (USR) seem to be the ones that effectively achieve the required feature. Such models are realised by a variety of potentials with features such as (near-)inflection points, a break, a bump or a dip in them [25–41] (see also [42] for a brief review of such potentials). There are also attempts at reconstructing this model using the characteristic behavior of the first slow roll parameter [43–47]. USR models while amplifying the scalar power, also lead to certain tell-tale features in the spectrum. Their scalar power spectrum contains a unique dip in the amplitude just prior to the sharp rise in power [48, 49]. The rise is typically of shape k^4 until the peak amplitude is achieved [43, 50, 51]. The shape post the peak is determined by the dynamics of inflation after the phase of USR.

The crucial aspects in such a spectrum are the location of the peak and the amount of enhancement of power over the typical nearly scale-invariant amplitude over large scales. These features are determined by the onset and duration of the USR phase during inflation. In the context of production of PBHs and secondary GWs, the location of peak dictates the mass of PBHs and the frequency of the peak amplitude in the spectral density of GWs, denoted as Ω_{GW} . The amount of enhancement in turn determines the population of PBHs

and the amplitude of Ω_{GW} at its maximum. Thus the onset and duration of USR have a direct impact on the characteristics of the relevant observables.

Since the onset of USR dictates the relevant mass of PBHs or frequency of GWs, it is usually tuned to values as per the desired range. The duration of USR is also tuned to achieve the required population fraction of PBHs or the amplitude of GWs. The production of PBHs is exponentially sensitive to the peak amplitude of scalar power, and therefore on the duration of USR. Hence, these parameters are fine-tuned in models that attempt to achieve significant fraction of PBHs along with secondary GWs.

There have been attempts in the literature to examine the consistency of models leading to enhanced power over small scales and constraints from CMB anisotropies over large scales. In Refs. [43, 46, 49, 52–57], there are discussions about the value of scalar spectral index and tensor-to-scalar ratio arising from such models over large scales and how they are often in tension with the CMB data. It is also noted that there can be strong running of spectral index when the enhancement in power is achieved closer to CMB scales [49]. Ref. [56] specifically focuses on a multi-field model of inflation and, using an analytical template of power spectrum, arrives at bounds on parameters of the two-field potential through a Markov-chain Monte-Carlo (MCMC) analysis against CMB dataset. However, there are no rigorous constraints on the models of USR through similar analysis. In this work, we attempt to constrain the dynamics of USR, particularly its onset and duration during inflation, using MCMC analysis against a variety of datasets over large scales.

Before the details of our analysis, we briefly summarize some of the key outcomes of the USR phase, based on the behavior of various inflationary potentials leading to USR. Over the course of about 70 e-folds of inflation, we need about four decades of CMB scales to have a nearly scale-invariant spectrum with reasonably small tensor-to-scalar ratio for agreement with Planck data. Hence we may expect just the initial 14–16 e-folds to have slow-roll dynamics during which these scales can evolve from sufficiently deep inside the Hubble radius and grow into the super-Hubble regime. This allows USR to occur anywhere in the last 55 e-folds of inflation. This essentially leaves a wide window of e-folds where USR can occur and last. On the other hand, a broad bound on the duration of USR comes from the limit on the enhancement of power spectrum $\mathcal{P}_s(k) < 1$. Since $\mathcal{P}_s(k) \propto \exp(6\Delta N)$ (ΔN denoting the duration in e-folds) during USR, this restricts the duration to be less than about three e-folds. Besides, if USR were to occur over an epoch that enhances power around scales of $k \sim 10^4 \text{ Mpc}^{-1}$, then the bound on $\mathcal{P}_s(k) < 10^{-5}$ from spectral distortions restrict USR to be less than 1.5 e-folds in this particular regime [58, 59]. Beyond these broad bounds, there are no strong constraints on the epoch of USR.

In this work, we attempt to directly constrain the epoch of the earliest onset of USR and its duration during inflation. To achieve this, we characterize the model of USR using a general parameterization of the first slow roll parameter over the entire course of inflation. This parameterization captures the essential features of USR models at the level of background and allows us to compute the dynamics of first-order perturbations. Moreover, it has explicit parameters that determine the onset of USR phase, its duration, and the smoothness of transition from SR to USR phase. We discuss the setup and details of this model in section 2. In section 3, we test our models against data on a range of scales, in particular the CMB and Lyman- α datasets. We first perform a comparison of model against the data of CMB anisotropies from Planck 2018 and BICEP/KECK 2015 missions. We then include the datasets of galaxy survey and supernova (SNIa) from BOSS, Pantheon 2018 and DES missions, along with CMB to inspect the improvement in the constraints. We observe that CMB anisotropy

data provide the essential bounds on the parameters and they are mildly improved by the later additions. We discuss this part of data analysis in section 3.1. To test our theoretical model against small-scale data, we use the evolution of effective optical depth from high spectral-resolution Lyman- α data [60]. The details of this method and the results of statistical comparison are given in section 3.2. Lastly, we discuss the crucial takeaways and outlook of our work in section 4.

2 Model of ultra-slow roll inflation

There are several potentials in the literature that achieve a brief epoch of USR during inflation (for a review of USR, refer [42]). These models have a phase where the canonical scalar field (inflaton ϕ) undergoes a phase of exponential decrease in the velocity in terms of e-folds N . Such dynamics of inflaton field is best studied through the behavior of the first slow roll parameter ϵ_1 . This parameter is defined with respect to the Hubble parameter H as

$$\epsilon_1(N) = -\frac{1}{H^2} \frac{dH}{dt}, \quad (2.1)$$

where t is the cosmic time. Using Friedmann equations in this case of inflation driven by a single canonical scalar field, it can be expressed as

$$\epsilon_1(N) = \frac{1}{2H^2} \left(\frac{d\phi}{dt} \right)^2 = \frac{1}{2} \left(\frac{d\phi}{dN} \right)^2. \quad (2.2)$$

Hence the phase of USR is defined by the exponential decrease of ϵ_1 in terms of e-folds N , contrary to the SR phase where it evolves much slowly.

A parameterization of $\epsilon_1(N)$ that captures this behavior suitably is convenient to understand the dynamics and also the corresponding effect on perturbations. There have been attempts at reconstruction of a brief epoch of USR during inflation, through parameterization of $\epsilon_1(N)$ in the literature [44, 45, 47]. Such parametric models of $\epsilon_1(N)$ are sought to generalize the dynamics of USR, without restricting to any specific potentials. We work with one such parametric model where the form of $\epsilon_1(N)$ is given by [42, 46]

$$\epsilon_1(N) = \frac{\epsilon_{1_i} e^{\epsilon_{2_i} N}}{2} \left[1 - \tanh \left(\frac{N - N_1}{\delta N_1} \right) \right] + \frac{\epsilon_{1_f}}{2} \left[1 + \tanh \left(\frac{N - N_1}{\delta N_1} \right) \right] + e^{\frac{N - N_e}{\delta N_e}}. \quad (2.3)$$

In this parametrization, the onset of USR is determined by N_1 and the smoothness of transition between USR and SR phases is determined by δN_1 . The duration of USR phase is controlled by ΔN which enters the model through ϵ_{1_f} , as we set $\epsilon_{1_f} = \epsilon_{1_i} \exp(-6 \Delta N)$. The onset and duration of USR, N_1 and ΔN , are the two essential parameters that we shall be varying to observe the effects on the scalar power over small scales. We set the value of smoothness to be $\delta N_1 = 0.31$. As we can see, our parametric model gives us a direct handle on the USR dynamics through the parameters N_1 and ΔN .

The transition to USR phase is effected at N_1 by the terms containing hyperbolic tangents. The value of ϵ_1 drops from ϵ_{1_i} to ϵ_{1_f} during the USR phase. Once it settles to ϵ_{1_f} , the final phase of SR begins and it lasts until the last term starts playing a role. The end of inflation is achieved by making ϵ_1 reach unity using the last term. We achieve 72 e-folds of inflation by setting $N_e = 72$ and the rapidity of the rise at the end is fixed as $\delta N_e = 0.55$.

The evolution of other background quantities such as the inflaton $\phi(N)$ and Hubble parameter $H(N)$ can be obtained from the behavior of $\epsilon_1(N)$ by inverting the relations (2.1) and (2.2) as

$$\phi(N) = \phi_i - \int_0^N dN' \sqrt{2\epsilon_1(N')} M_{\text{Pl}}, \quad (2.4)$$

$$H(N) = H_i \exp \left[- \int_0^N dN' \epsilon_1(N') \right], \quad (2.5)$$

along with suitable choice of initial conditions for respective quantities, namely the field value ϕ_i and the Hubble parameter H_i . The shape of the potential $V(\phi)$ can also be obtained from the behavior of $\phi(N)$ and $V(N) = [3 - \epsilon_1(N)] H^2(N) M_{\text{Pl}}^2$.

We numerically evolve the scalar and tensor perturbations over the background that is modelled through $\epsilon_1(N)$ and compute the corresponding spectra close to the end of inflation, well past the epoch of USR. The dimensionless power spectra of the scalar and tensor perturbations are defined, in terms of the associated mode functions f_k and g_k respectively, as [61–65]

$$\mathcal{P}_s(k) = \frac{k^3}{2\pi^2} |f_k|^2, \quad (2.6)$$

$$\mathcal{P}_T(k) = 4 \frac{k^3}{2\pi^2} |g_k|^2. \quad (2.7)$$

The pivot scale $k_p = 0.05 \text{ Mpc}^{-1}$ is set to exit the Hubble radius 50 e-folds before the end of inflation, i.e., at $N_p = 22$ in our parametrization. Thus the scales of CMB $k = [10^{-4}, 1] \text{ Mpc}^{-1}$ are set to exit the Hubble radius during $N = [16, 25]$ of our model. To relate to the convention of counting e-folds from the end of inflation, let us define

$$\bar{N} = N_e - N, \quad (2.8)$$

which in our case becomes $\bar{N} = 72 - N$. Thus, in terms of \bar{N} , the pivot scale exits Hubble radius at $\bar{N} = 50$ and the range corresponding to CMB scales is $\bar{N} = [56, 47]$. We shall use \bar{N} in later analysis, when we interpret various bounds on e-folds.

The behavior of scalar power spectrum for the range of parameters we work with is presented in Fig. 1. We observe that our model of $\epsilon_1(N)$ captures the essential features of the spectra arising from a generic model of USR achieved using a potential. The scalar power spectrum contains the signatures of USR such as the dip, followed by the rise of k^4 , and a peak amplitude. Since our model has an extended duration of SR after USR, the spectrum settles to another scale invariant regime past the peak. These individual features have been studied in several earlier works [43–45, 48, 50, 51, 55, 66–69].

As mentioned earlier, since we are interested in enhancing scalar power over small scales, the first phase of SR corresponds to the time when CMB scales exit the Hubble radius. The dynamics of this phase is determined by the prefactor in the first term of Eq. (2.3), involving $\epsilon_{1i}, \epsilon_{2i}$. It is modelled to ensure proper values for the overall amplitude of the spectrum A_s , scalar spectral index n_s and tensor-to-scalar ratio r over scales exiting in the initial regime of SR. We choose $\epsilon_{1i} = 1.5 \times 10^{-4}$, $\epsilon_{2i} = 3.5 \times 10^{-2}$, along with the initial value of the Hubble parameter $H_i = 7.3 \times 10^{-6} M_{\text{Pl}}$, such that we obtain $A_s = 2.12 \times 10^{-9}$, $n_s = 0.96$ and $r = 5.04 \times 10^{-3}$, which are well in agreement with the constraints on these parameters from CMB. We discuss our choice of these parameters in detail in App. A. Further, we also

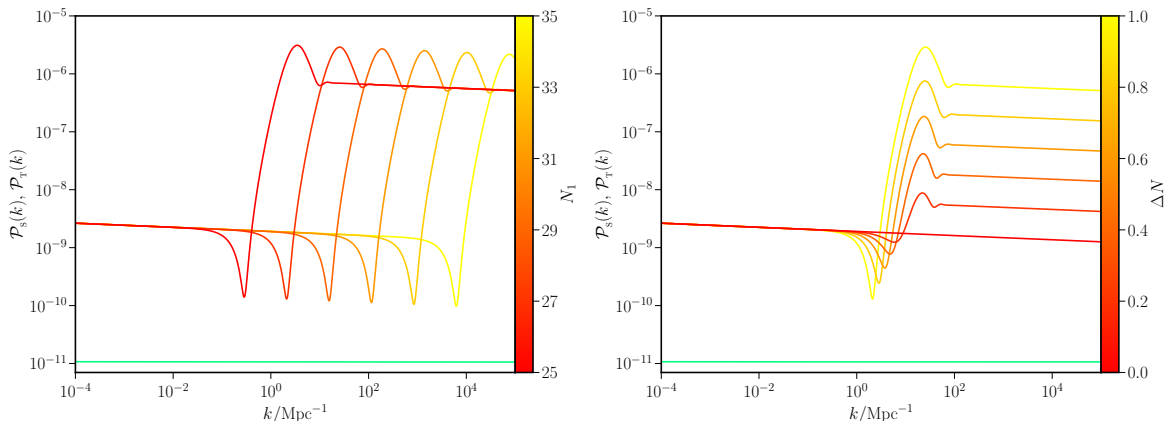


Figure 1. We present the behavior of scalar power spectra (in shades of red to yellow) arising from the parametric model of USR with variation of the two parameters of interest: the onset of USR N_1 (in the left panel, with constant $\Delta N = 1$) and the duration of USR ΔN (in the right panel, with constant $N_1 = 27$). The location of enhancement of scalar power is determined by N_1 with larger values implying enhancement over smaller scales. The amplitude of enhancement is determined by ΔN with large values implying large enhancement. The range of parameters are chosen such that we preserve the nearly scale invariant behavior over $k \leq 0.1 \text{ Mpc}^{-1}$ and also ensuring that we do not violate the upper bound on enhancement due to CMB spectral distortions over scales around $k \simeq 10^4 \text{ Mpc}^{-1}$. The tensor power spectrum remains unaffected by the USR dynamics and stays the same across variation of parameters. It is displayed as a single horizontal green line.

restrict the range of variation of ΔN so that the enhancement does not violate the bound on $\mathcal{P}_s(k)$ due to spectral distortions in CMB around $k \simeq 10^4 \text{ Mpc}^{-1}$. As we vary the parameter N_1 we observe that feature of dip and rise shift across the range of wavenumber k , with larger values of N_1 shifting it to larger values of k . The increase in ΔN leads to increase in the amplitude of enhancement while also making the dip more prominent prior to the rise.

The tensor power spectrum remains nearly scale invariant throughout the range of scales, as it is largely unaffected by USR dynamics. However, they may suffer a step like drop in amplitude in case of models that have a brief rise in $\epsilon_1(N)$ just prior to the epoch of USR. Such models may even lead to an interruption in inflation if the rise in $\epsilon_1(N)$ crosses unity before decreasing rapidly during USR. These models are called punctuated inflationary models [70–73]. We do not include such a punctuation in our parametric model as we are mainly interested in the rise in the scalar power, though it can be included if required through an additional term in the parameterization (see Ref. [46] for such a reconstruction).

Based on our analysis, we obtain the following relation between the number of e-folds N_1 and the scale corresponding to the peak of the primordial power spectrum, k_{peak} (Figure 1). For $\Delta N = 0.2$,

$$N_1 \simeq 25 + \ln \left(\frac{k_{\text{peak}}}{3 \text{ Mpc}^{-1}} \right) \quad (2.9)$$

and

$$N_1 \simeq 25 + \ln \left(\frac{k_{\text{peak}}}{3.48 \text{ Mpc}^{-1}} \right) \quad (2.10)$$

for $\Delta N = 1$. From Figure 1 it is clear that the power spectrum deviates significantly from the nearly scale invariant behavior over $k \gtrsim k_{\text{peak}}/10$.

Parameters	Minimum	Maximum
$\Omega_b h^2$	5×10^{-3}	0.10
$\Omega_c h^2$	10^{-3}	0.99
$100 \theta_{MC}$	0.50	10.00
τ	10^{-2}	0.80

Table 1. The priors on the standard cosmological parameters that are used while comparing the models against datasets of Planck 2018, BK15, BOSS, Pantheon 2018 and DES are listed.

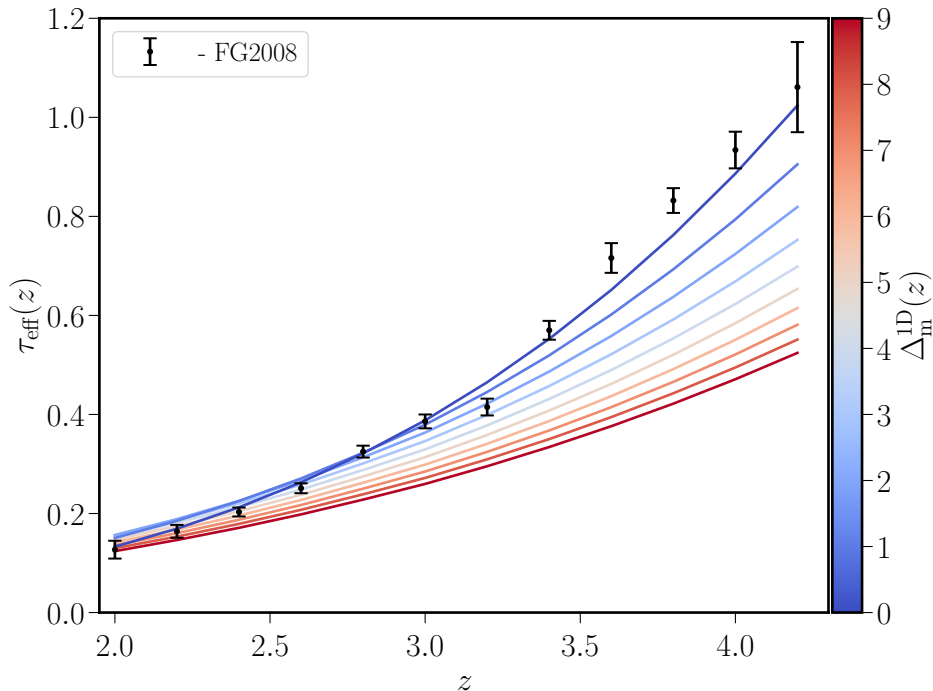


Figure 2. The evolution of τ_{eff} is shown based on our model predictions along with the high spectral-resolution data (in black dots along with error bars, FG2008) [60]. Different curves (from top to bottom) correspond to increasing average relative difference of 1D power spectrum $\Delta_m^{1D}(z)$ [cf. Eq. (3.4)] (in shades of blue to red). In simulating the evolution of $\tau_{\text{eff}}(z)$ for different values of $\Delta_m^{1D}(z)$, the Lyman- α parameters have been held fixed to the following values: $J_0 = 10^{-12} \text{ s}^{-1}$, $T_0 = 2.3 \times 10^4 \text{ K}$ and $\gamma = 0.7$.

We use this parametric model of USR and the associated numerical setup that computes scalar and tensor power spectra to compare against the datasets of CMB, SNIa, galaxy surveys and Lyman- α . We shall discuss the methods and results of our analyses in the following sections.

3 Results

In this paper, we aim to constrain the deviation of a class of USR models from the standard model of slow roll inflation followed by Λ CDM evolution. Planck CMB temperature and polarization data puts strong constraints on such deviation at scales $10^{-3} \text{ Mpc}^{-1} \lesssim k \lesssim$

0.2 Mpc^{-1} ¹. Lyman- α data at intermediate redshifts ($2 \lesssim z \lesssim 4$) can probe scales comparable to the Jeans' scales in IGM ($k_J \simeq 10 \text{ Mpc}^{-1}$). We consider Planck data and other related datasets at comparable scales, along with high spectral-resolution Lyman- α data in our analysis.

3.1 CMB, SNIa and galaxy survey data

We consider the combined dataset of anisotropies in temperature and polarization of CMB from Planck 2018 and BICEP/KECK 2015 (BK15), along with galaxy survey dataset from BOSS, Pantheon 2018 and DES [74–78]. Given the sensitivity of the CMB data, we expect the strongest constraint on the model parameters from Planck data. Hence, we first compare the model against the data of Planck 2018 and BK15, and examine the constraints. We then extend the datasets to include BOSS, Pantheon 2018 and DES to study the improvement in the constraints. We use the publicly available package called CosmoMC to perform the comparison and Monte-Carlo sampling of the posterior distribution of parameters [79]. We modify the CAMB package within the setup of CosmoMC to incorporate the power spectra arising from the model of interest [80]. We use a modified version of a package called PBS², which computes scalar and tensor power spectra for a given model of inflation, to implement the above mentioned alteration to CAMB in CosmoMC. Further, we use GetDist to marginalize along various dimensions in the parameter space and plot the resulting posterior distribution [81].

Since we are interested in studying the impact of enhanced scalar power on small scales, we set the priors on the parameters of interest as $N_1 = [25, 35]$ and $\Delta N = [0, 1]$. The parameter N_1 determines the location of the enhancement of the scalar power spectrum and the range of values that we have chosen corresponds to onset of enhancement over $k = [0.1, 10^5] \text{ Mpc}^{-1}$ ³.

The parameter ΔN affects both the location and amount of enhancement of the spectrum. Our choice of the range corresponds to relative enhancement of about $[0, 10^3]$ over the nearly scale-invariant amplitude. As noted in Sec. 2, we choose the range of ΔN such that we do not violate the upper bound on $\mathcal{P}_s(k) \lesssim 10^{-5}$ arrived at from the limit on spectral distortions obtained by FIRAS [58, 59, 82]. The amplitude of the scalar and tensor power over the large scales prior to enhancement is determined by H_1 , ϵ_{1_1} and ϵ_{2_1} . Since they are fixed at constant values as mentioned in Sec. 2, the overall amplitudes of scalar and tensor power are not varied during the comparison against data. The choice of the values of these three parameters have been motivated in App. A, along with a separate analysis that relaxes this assumption. The priors on the other standard cosmological parameters are given in Tab. 1.

We first compare the model against the CMB datasets by using the likelihoods of Planck2018+BK15. We obtain the posterior distribution of the cosmological parameters from this analysis and present their marginalized contours in Fig. 3. We present the contours of these parameters from Λ CDM model with the standard power-law forms of primordial scalar and tensor power spectra (PL model), along with our model's contours for comparison. Firstly, we observe that four of the six cosmological parameters, namely $\Omega_c h^2$, $\Omega_b h^2$, θ_{MC} and τ are constrained around the same value as they are in PL model. We note that the

¹The approximate smallest scale probed by Planck data corresponds to $k \simeq \ell/\eta_0$, where $\ell \simeq 2500$ and the conformal time at the present time $\eta_0 \simeq 11000 \text{ Mpc}$

²It is developed by one of the authors and publicly available at <https://gitlab.com/ragavendrahv/pbs>.

³We should clarify we are not allowing for an epoch of USR at a much earlier time during inflation, which along with rescaling of the overall normalization, can suppress power over the largest scales probed by CMB, $k \simeq 10^{-4} \text{ Mpc}^{-1}$. In fact, it has been shown that such an epoch can mildly improve the fit to CMB [72, 73]. However, we are not allowing for this effect in our work and the priors on N_1 are chosen solely to explore only the small-scale enhancement due to a late epoch of USR.

constraints on τ are much tighter in our model compared to the usual case. This is because τ is degenerate with the overall normalization and we have lifted this degeneracy by fixing of the values of H_1 , ϵ_{1_i} and ϵ_{2_i} in our model, which fix the overall normalization. We address this issue in the App. A where we allow these parameters to vary.

From posterior distribution, it is clear N_1 is bounded from below. To further quantify this lower limit, we use `GetDist` which deals with one-sided distributions and sharp boundaries in the distribution using a linear boundary kernel estimator and suitable normalization [81]. We obtain $N_1 > 28.90$ at $1\text{-}\sigma$ level and $N_1 > 26.71$ at $2\text{-}\sigma$ level. On the other hand, ΔN is unconstrained.

Next, we extend the dataset to include SNIa and galaxy survey, i.e. `BOSS`, `Pantheon 2018` and `DES` likelihoods. We present the marginalized contours of the posterior distribution in Fig. 4. We once again observe that the parameters such as $\Omega_c h^2$, $\Omega_b h^2$ get constrained around the same values as in the PL model. Using `GetDist` we find that N_1 lies in the range $28.86 < N_1 < 33.98$ at the level of $1\text{-}\sigma$ and $N_1 > 27.53$ at the level of $2\text{-}\sigma$. ΔN is again unconstrained, though there is mild preference towards $\Delta N = 0$.

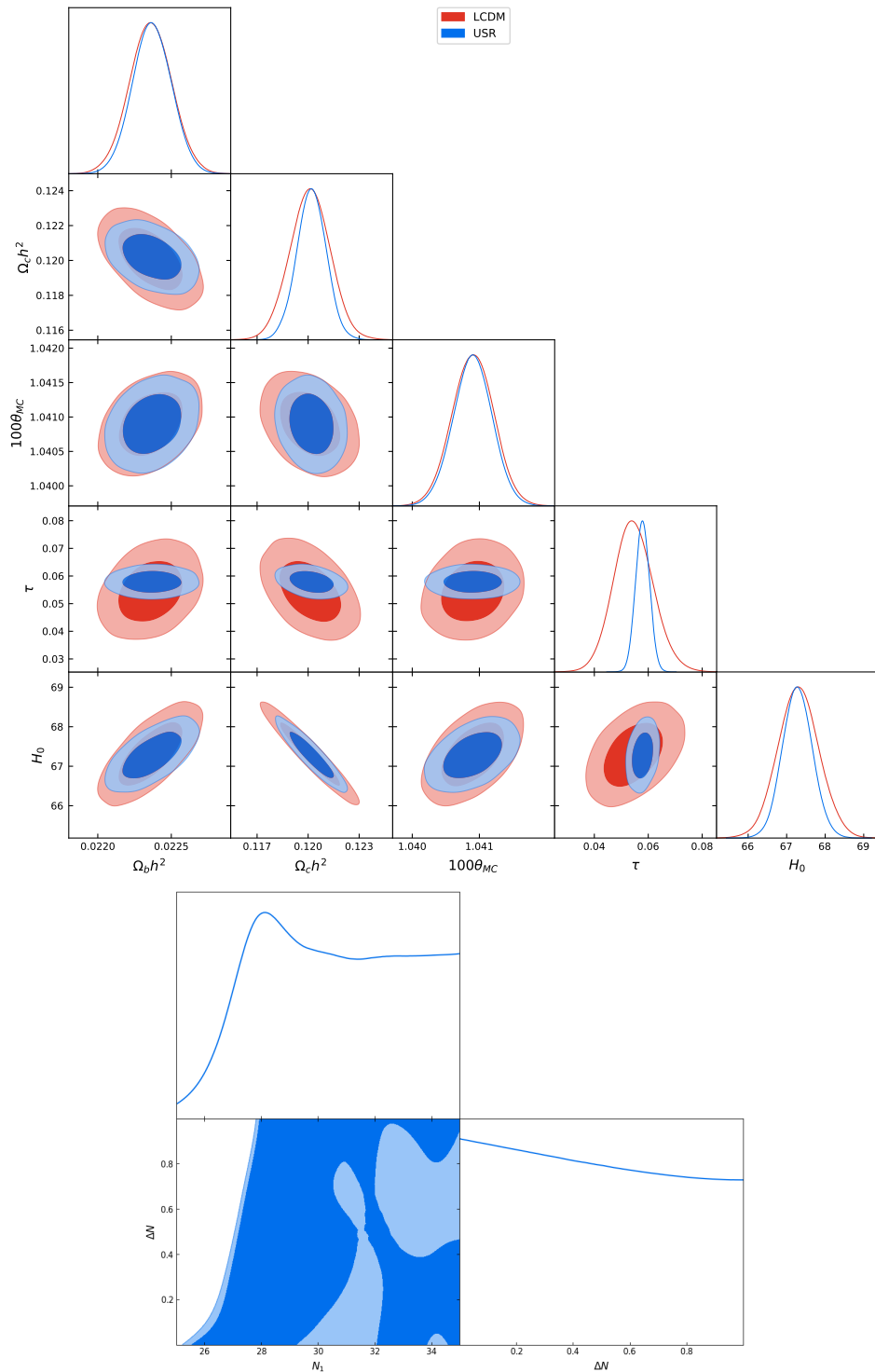


Figure 3. The 1- σ and 2- σ contours of the posterior distributions of the four standard cosmological parameters and a derived parameter H_0 , when compared against CMB datasets Planck2018+BK15 are displayed in the top panel. We overlay the contours arising from the two models: the standard Λ CDM model with the nearly scale-invariant primordial power spectra (in red) and the model of USR (in blue). The distributions of parameters describing USR models, N_1 and ΔN are presented in the bottom panel. The other model parameters of the inflationary epoch are set to the values mentioned in the text.

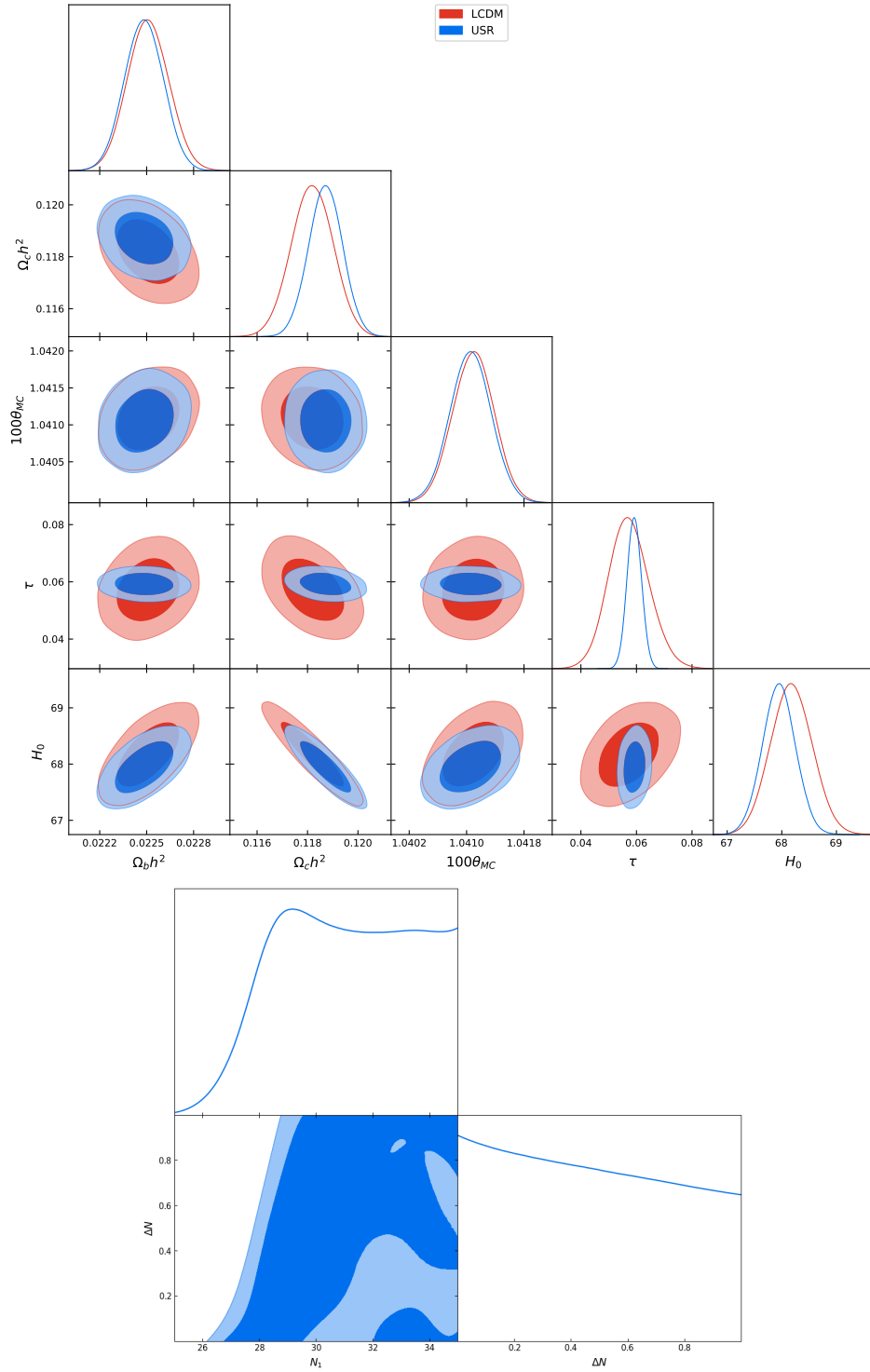


Figure 4. The same as Fig. 3 except the contours correspond to comparing our theoretical models against additional data sets: Planck2018+BK15+BOSS+Pantheon18+DES

The lower bound obtained on N_1 is an important result of this analysis. It translates to an upper bound on \bar{N}_1 , the earliest onset of USR from the end of inflation. The bound of $N_1 > 27$ is simply $\bar{N}_1 < 45$, implying that USR can occur only in the last 45 e-folds of inflation. It essentially indicates the data's preference for the nearly scale-invariant spectrum up to scales $k \lesssim 1 \text{ Mpc}^{-1}$ and avoidance of any deviation such as a dip or rise over these scales. On the other hand, the indifference of data towards the range of ΔN suggests that an epoch of USR lasting for as long as 1 e-fold beyond $N_1 = 27$ and hence a relative enhancement as large as 10^3 past $k = 1 \text{ Mpc}^{-1}$ does not affect the fit of the model over large scales. We note that this scale is comparable to but smaller than our expectation based on using the relation $k\eta_0 = \ell$, which follows from the property of spherical Bessel function. We note that for a given angular scales ℓ , the contribution from a linear scale $k < \ell/\eta_0$ falls very sharply. However, it only falls as $1/(k\eta_0)$ for $k > \ell/\eta_0$ (for details see e.g. [83]). This means CMB data is sensitive to much larger values of k for a fixed ℓ and η_0 as our results show.

3.2 Lyman- α forest

Lyman- α forest is the dense, ragged forest of lines seen in the spectra of the background quasars. These lines correspond to regions in the Inter-Galactic Medium (IGM) with HI column number density lying between the range: $N_{\text{HI}} = 10^{12} - 10^{15} \text{ atoms/cm}^2$. Hydrodynamical simulations identify these regions with underlying matter densities in the mildly non-linear range ie. $\delta \leq 10$. It is known that Lyman- α forest can probe density perturbations on scales as small as the thermal Jeans' scale of IGM at intermediate redshifts ($k \simeq 10 \text{ Mpc}^{-1}$). Based on hydrodynamical simulation of Lyman- α forests, Murgia et al. [84] put constraints on a large range of models with matter power deficit as compared to the Λ CDM model. Most of the models we consider correspond to excess power as compared to the Λ CDM model. While it is tempting to use the results of [84] to constrain our models, the relevant cosmological observable in this case, the flux deficit, is a non-linear function of matter power and therefore we recompute these constraints based on a semi-analytic approach [85–89].

The semi-analytic modelling of Lyman- α has been used to constrain cosmological models which either have excess or reduced matter power in [88, 89]. In this approach, the observed redshift evolution of effective optical depth of Lyman- α forest, based on high spectral-resolution data [60], is used.

To constrain our model against the Lyman- α data, we define and use the relative difference between the 1D baryonic power spectra of the models of interest $\mathcal{P}_b^{\text{1D}}(k)$ and the standard Λ CDM evolution following slow-roll inflation leading to a power-law primordial power spectrum $\mathcal{P}_b^{\text{1D}}(k)|_{\text{PL}}$. The 1D baryonic power spectrum can be defined in terms of the 3D baryonic power spectrum $P_b^{(3)}(k, z)$ as (e.g. [85, 86] for details):

$$P_b^{(1)}(k, z) = \frac{1}{2\pi} \int_{|k|}^{\infty} k' P_b^{(3)}(k', z) dk' \quad (3.1)$$

with

$$P_b^{(3)}(k, z) = \frac{P_m^{(3)}(k)}{[1 + (k/k_J)^2]^2}, \quad (3.2)$$

and the Jeans wavenumber k_J is:

$$k_J = H_0 \left[\frac{2\gamma k_B T_0}{3\mu m_p \Omega_m (1+z)} \right]^{-1/2}, \quad (3.3)$$

where the parameters have their usual meaning, with $\mu = 0.6$. For the standard choice of parameters, we have $k_J \simeq 8.5 h \text{ Mpc}^{-1}$ at the redshift $z = 3$.

We further average the relative difference $\Delta_m^{1D}(k)$ between 1D baryonic power spectra over the range of k . This allows us to define Δ_m^{1D} as follows:

$$\begin{aligned}\Delta_m^{1D}(k, z) &= \frac{\mathcal{P}_b^{1D}(k, z) - \mathcal{P}_b^{1D}(k, z)|_{\text{PL}}}{\mathcal{P}_b^{1D}(k, z)|_{\text{PL}}}, \\ \Delta_m^{1D}(z) &= \frac{1}{\int d \ln k} \int d \ln k \Delta_m^{1D}(k, z).\end{aligned}\quad (3.4)$$

We note that $\Delta_m^{1D}(z)$ is a function of redshift owing to the evolution of Jeans scale (Eq. (3.3)). To parameterize the relative difference, $\Delta_m^{1D}(z)$ is computed at the redshift of $z_* = 2.2$. The choice of z_* has no impact on our main results. The range of integration over k is taken to be $[10^{-5}, 10^3] \text{ Mpc}^{-1}$ to arrive at $\Delta_m^{1D}(z_*)$. Our approach is similar to Murgia et al. (2017) [84] where the deviation from the standard 1D power spectrum is quantified and compared against data. We differ from the measure used by [84] in using baryonic power spectra and using a larger range of k to define the relative difference between the standard and modified models. We use a semi-analytic model for probing the thermal, dynamical and ionization state of the Lyman- α clouds at higher redshifts using the following parameters: J_0 (the intensity of hydrogen-ionizing photons), T_0 (the temperature of the IGM), γ (the equation of state of the Lyman- α clouds) (for details see [89] and references therein). Based on observational data and hydrodynamical simulations, these parameters are varied in the following range: $7000 \leq T_0 \leq 15000 \text{ K}$, $0.7 \times 10^{-12} \text{ sec}^{-1} < J_0 < 2 \times 10^{-12} \text{ sec}^{-1}$, and $0.9 \leq \gamma \leq 2.2$ (for details see [89]). In addition, two cosmological parameters, N_1 and ΔN , denoting the modified small scale power owing to USR phase, are included in the analysis.

We have simulated the 1D density and velocity field using lognormal distribution in the redshift interval $2 \leq z \leq 4.2$ at uniform redshift intervals of $\Delta z = 0.1$ for comparison with data. The Lyman- α effective optical depth $\tau_{\text{eff}}(z)$ is defined as: $\tau_{\text{eff}}(z) = -\log [\langle \exp(-\tau) \rangle]$. From the standpoint of observation, the ensemble average (represented by the angular brackets $\langle \dots \rangle$) is substituted by the average over the number of individual Lyman- α clouds at a particular redshift: $\tau_{\text{eff}}(z) = -\log [\sum_i \exp(-\tau_i)/N]$, where N is the number of the simulated Lyman- α clouds at a redshift z , and τ_i denotes the optical depth of the i -th Lyman- α cloud at that redshift.

In Figure 2, we plot the evolution of τ_{eff} along with the data. To understand the evolution of τ_{eff} , we first discuss two extreme cases. If $\tau_i \ll 1$ for all clouds, then $\tau_{\text{eff}} \propto (1+z)^{4.5}$, which is the expected evolution of the Gunn-Peterson optical depth for the background universe. In the other extreme case, if $\tau_i \gg 1$, then τ_{eff} is independent of τ_i and hence of redshift. The observed behaviour lies between these two extremes which shows that many clouds are making transition to optical thin to optically thick as redshift increases. ($\tau_i = N_{\text{HI}} \sigma_\alpha$, where σ_α is the cross-section of Lyman-alpha scattering. The line center cross-section $\simeq 5 \times 10^{-14} \text{ cm}^{-2}$ for $T_0 \simeq 10^4$.) The data fits the Λ CDM model well and can be used to constrain models with deficit or excess power [88]. Figure 2 shows the redshift evolution of τ_{eff} get flatter as the matter power is increased. This is expected as a larger fraction of Lyman- α clouds become optically thick at higher redshift as the matter power is increased. This demonstrates that the slope of the τ_{eff} evolution is a robust probe of matter power (for further details see [88, 89] for cases analysing both deficit and excess of power). However, the effective optical depth is also affected by parameters used to model the ionization and thermal state of clouds. In particular, the increase in matter power is degenerate with ionizing intensity J_0 and partially

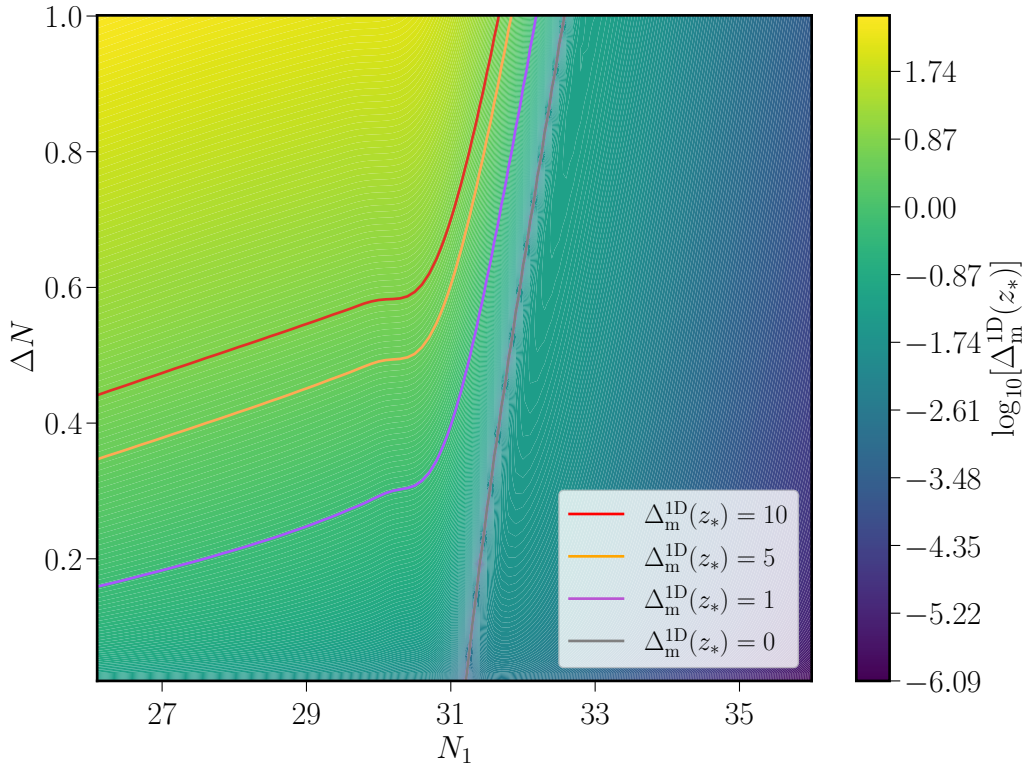


Figure 5. We present the density plot of the average relative difference of the 1D matter power spectrum of the USR model with respect to the standard power law power spectrum $\Delta_m^{1D}(z_*)$ (Eq. (3.4)), as a function of N_1 and ΔN (in shades of blue to green). We have also highlighted the contours corresponding to $\Delta_m^{1D}(z_*) = 10, 5, 1$ and 0 (with lines in red, orange, violet and grey respectively). In the region to the right of the line corresponding to $\Delta_m^{1D}(z_*) = 0$, the parameters lead to $\Delta_m^{1D}(z_*)$ being small and negative in value.

degenerate with T_0 and γ (see [89] for details). Therefore, the magnitude of the change of matter power that can be probed by the data depends on the prior information on these parameters. We discuss the priors on these parameters above. These correspond to the widest possible priors on these parameters from the literature. Based on our analysis of the simulated data, we find that these priors constrain the change in the 1D matter power spectrum to be smaller than roughly a factor of five. For narrower priors, the constraints are stronger. If the results of [84] are directly applied to our case, the change in the matter power is constrained to be less than approximately 50%.

In Fig. 5, we present the constraints from Lyman- α data as a color gradient map with contours based on the deviation measure, $\Delta_m^{1D}(z_*)$, in the N_1 - ΔN plane. The contours denoting the values of $\Delta_m^{1D}(z_*) = 1, 5$ and 10 are displayed. The region above these contours is ruled out. To understand these constraints, we show models corresponding to two values of $\Delta_m^{1D}(z_*)$ in Fig. 6. In Fig. 5 we also plot a curve corresponding to $\Delta_m^{1D}(z_*) = 0$. This curve demarcates the region of positive deviation from negative deviation. The negative deviation is caused by 1-D spectrum getting suppressed by the dip in matter power and the subsequent rise suppressed by the cutoff at Jean's scale [cf. Eq. (3.2)]. However, all the spectra that

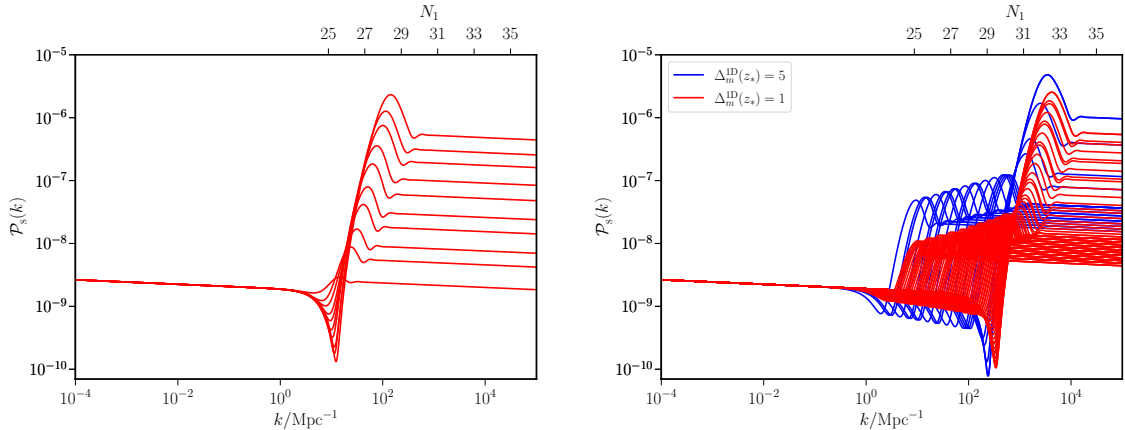


Figure 6. Left Panel: The scalar power spectra based on $2\text{-}\sigma$ bound on parameters N_1 and ΔN from CMB and other related data sets (Planck2018+BK15+BOSS+Pantheon18+DES) are shown (cf. Fig. 4). Right Panel: The matter power spectra corresponding to constraints from Lyman- α data are displayed. The scalar power spectra leading to $\Delta_m^{1D}(z_*) = 1$ and $\Delta_m^{1D}(z_*) = 5$ are presented (in red and blue respectively). These spectra are obtained from the values of N_1 and ΔN along the respective contours in Fig. 5. The upper x-axis displays N_1 corresponding to the location of the peak, k_{peak} , in the spectrum. It is obtained using the relation: $N_1 \simeq 25 + \ln(k_{\text{peak}}/\text{Mpc}^{-1}) - \ln(3.48)$ (cf. Eq. (2.10))

we consider (Fig. 6) yield only a small negative deviation, $|\Delta_m^{1D}(z_*)| \leq 10^{-2}$. The data is insensitive to such small deviation and therefore cannot probe the interplay between the dip and subsequent rise in the matter power (Fig. 6). Fig. 5 implies that significant duration of USR $\Delta N \geq 0.5$, can occur only for $N_1 > 31$, or equivalently $\bar{N}_1 < 41$. This means that substantial rise in power can occur only at $k \geq 10^2 \text{Mpc}^{-1}$.

We can understand our results using Eqs. (3.2), (3.1), and (3.3). In the usual ΛCDM model based on PL power spectra from slow roll inflationary models, the three-dimensional matter power spectrum scales as $k^{-3}(\log(k))^2$ at small scales (see e.g. [83]). For $k \lesssim k_J$, the baryonic 1D power spectrum scales as $k^{-1}(\log(k))^2$ and for $k > k_J$, $P_b^{(1)}(k, z) \propto k^{-5}(\log(k))^2$. In the USR models, the increase in the primordial power spectrum can scale as k^4 (e.g. Fig. 1). This means the main contribution to the enhanced power comes from scales $k \lesssim k_J \simeq 10 \text{Mpc}^{-1}$ as the 1D baryonic power spectrum scales as $k(\log(k))^2$ for $k < k_J$. However, for $k > k_J$ the decrement in 1D power spectrum is shallow ($P_b^{(1)}(k, z) \propto k^{-1}(\log(k))^2$) and we expect non-negligible contribution from smaller scales. Our analysis suggests scales up to 10 times smaller than $k = k_J$ can be constrained in USR models as the 1D power spectrum falls by only a factor of two in this range: $P_b^{(1)}(100, z)/P_b^{(1)}(10, z) \simeq 0.5$.

4 Conclusion

Recent LIGO and PTA discoveries have opened the possibility of enhanced scalar power at small scales. This enhancement can be achieved by a brief USR phase during the inflationary era. In this paper, we aim to detect/constrain the dynamics of this phase of inflation using cosmological data. In particular, we use CMB data owing to its unprecedented precision and Lyman- α data as it is sensitive to small scales. We parameterize our models to determine the onset of the USR phase during inflation and the deviation of the matter power as compared to the power-law model.

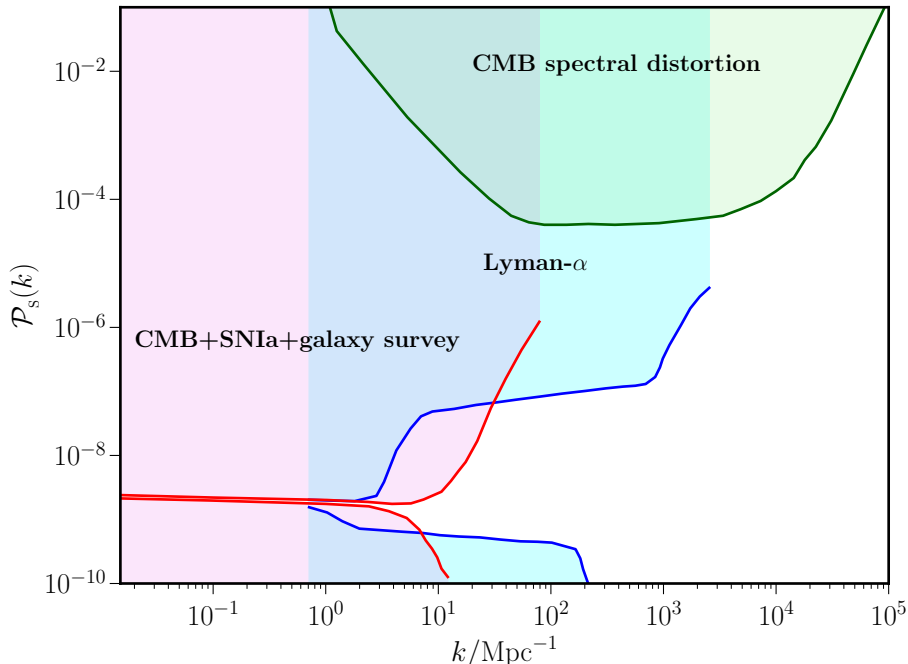


Figure 7. The constraints shown in Fig. 6 are displayed in $\mathcal{P}_s(k)$ - k plane. The red and blue lines correspond to CMB+SNIa+galaxy surveys and Lyman- α data, respectively. The region bounded by these lines, e.g. narrow band around $\mathcal{P}_s(k) \simeq 2 \times 10^{-9}$, is allowed. The red lines demarcating the allowed region correspond to the envelopes of power spectra presented in the left panel of Fig. 6, which in turn is obtained from the $2\text{-}\sigma$ contour in the N_1 - ΔN plane in Fig. 4. The blue lines bounding the allowed region are the envelopes of power spectra presented in the right panel of Fig. 6. We have taken the set of spectra which lead to an average relative difference $\Delta_m^{\text{1D}}(z_*) = 5$. The three bands, from left to right, correspond to the region of spectrum ruled out by CMB+SNIa+galaxy surveys data (lighter shade of red), both CMB+SNIa+galaxy surveys (in light blue), and by Lyman- α data (shaded in cyan). We also display the constraints from CMB spectral distortion (green lines bounding the region in lighter shade of green). For details see e.g. [82].

From CMB and other data at comparable scales, we find that the earliest onset of USR can only be $\bar{N}_1 \lesssim 45$ (Figs. 3 and 4 for two USR parameters and Fig. 8 for two USR parameters in addition to three SR parameters). With Lyman- α dataset, the onset gets pushed further to $\bar{N}_1 \lesssim 41$ (Fig. 5). The duration ΔN is largely unconstrained from CMB and other datasets. But Lyman- α strongly constrains the duration to be $\Delta N \lesssim 0.4$ along with $\bar{N}_1 < 41$. These constraints limit the possibility of having any appreciable epoch of USR only to the last 41 e-folds of inflation. This implies a constraint on the amplitude of $\mathcal{P}_s(k) < 10^{-7}$ over $0.1 < k/\text{Mpc}^{-1} < 10^2$. Such a constraint is a considerable improvement of about two orders of magnitude on the bound on $\mathcal{P}_s(k)$ compared to the limit from FIRAS over these scales [82].

In Fig. 6, we plot the range of power spectra that are allowed by different data sets. In Fig. 7, we present our constraints in terms of the primordial power spectrum and wavenumber, which is more readily connected to cosmological observables and can be compared to other constraints such as spectral distortion. This helps us see the improvement in the constraint on the amplitude of power by Lyman- α data over spectral distortion for $k \lesssim 10^2 \text{ Mpc}^{-1}$. We should add that the exact shape of the bounds, especially the blue lines corresponding to

Lyman- α constraints in Fig. 7, are dictated to some extent by the shape of the spectrum in the USR model of interest. (e.g. [90, 91] for similar constraints but for different models of dark matter and specific parameterized forms of the primordial power spectra.)

In light of our constraint on the onset of USR, we should remark about the implications of USR phase for other cosmological datasets and the possibility of extending these constraints using future observations.

1. As mentioned earlier, the dip in power prior to rise is a unique signature of USR models. In an earlier work, it was shown that this dip could be gleaned in the spectrum of 21-cm signals from the Dark Ages [49]. Due to the constraint that we have obtained on \bar{N}_1 and ΔN , if the dip were to occur at $k \simeq 10 \text{ Mpc}^{-1}$, it shall be shallower, with the amplitude at the lowest point within an order of magnitude of the nearly scale-invariant behavior. Else it may occur deeper but only at $k \geq 10^2 \text{ Mpc}^{-1}$.
2. To constrain the onset of USR at even smaller scales, one needs to explore possible future constraints due to spectral distortions over the scales of $10^4 \text{ Mpc}^{-1} \lesssim k \lesssim 10^6 \text{ Mpc}^{-1}$. We have already accounted for the constraint due to FIRAS on $\mathcal{P}_s(k) \lesssim 10^{-5}$ by restricting the range of duration of USR to be $\Delta N < 1$. But an upcoming mission like PIXIE with sensitivity as strong as $\mathcal{P}_s(k) \sim 10^{-8}$ can strengthen our constraints on \bar{N}_1 and ΔN [92]. Conversely the detection of spectral distortion of such levels, could be a confirmation of a brief USR phase.
3. As noted in the foregoing, there have been attempts to explain the stochastic GWs detected by PTA using USR models [19, 20, 24]. A scalar power spectrum that is required to induce such a secondary GW spectrum should have its steep rise in power between $10^5\text{--}10^7 \text{ Mpc}^{-1}$. This in turn corresponds to a phase of USR beginning at about $\bar{N}_1 \leq 32$. Such a value is still in the viable range of \bar{N}_1 as per the bounds we have obtained. If the signal by PTA is indeed due to USR, then it provides a crucial insight into the onset and duration of USR phase during inflation. However, we should caution that such a steep enhancement in power is beget along with strong scalar non-Gaussianity, captured in a non-trivial behavior in the associated non-Gaussianity parameter f_{NL} [42]. One needs to be careful in accounting for the non-Gaussian contributions to Ω_{GW} while comparing USR models against GW datasets [93–109].
4. The discovery of many high-redshift galaxies with unusually high stellar mass by JWST (e.g. [110, 111]) could be pointing at cosmological models with more power at small scales as compared to the Λ CDM model. However, it is also likely that the observed behaviour is owing to much higher star formation efficiency at high redshifts with significant contribution from population III stars (e.g. [110] and references therein). This issue is still being debated and remains unsettled.

In this paper, we consider the tree-level contribution to the primordial power spectrum. For USR models, there is ongoing discussion in the literature about the possibility of higher-order (loop-level) contribution dominating over the tree-level primordial power spectrum (e.g. [112–118] and [119–122] for counter claims). Within the framework of this ongoing debate, such an effect is possible only in the following cases: (i) the transitions between SR and USR are near-instantaneous and (ii) the enhancement in power is such that $\mathcal{P}_s(k) \sim 10^{-2}$, as required in the context of production of PBHs. This is not the case in our model as the transitions are not instantaneous, but smooth as is the case in any realistic model of USR

driven by a smooth potential. Also, the range of ΔN we have worked with is restricted such that the maximum amplitude of $\mathcal{P}_s(k) \leq 10^{-5}$ as we do not violate the bound due to spectral distortion. Hence, the argument of loop-level spectrum dominating over tree-level spectrum does not occur in our analysis.

Acknowledgements

The authors acknowledge the usage of high-performance computing cluster at Raman Research Institute for various numerical computations. HVR thanks Raman Research Institute for support through postdoctoral fellowship.

A Choice of parameters determining spectra over large scales

As mentioned in Sec. 2, we have fixed the values of certain parameters of USR model during our analysis against data. In this appendix we provide justification for the choice of values of those parameters. We relax the fixed values on H_i , ϵ_{1i} and ϵ_{2i} , and vary them against CMB data with suitable priors, along with N_1 and ΔN to arrive at best fit values and constraints on them. We find that the values we have worked with in Sec. 2 are consistent with these constraints.

To begin with let us focus on the part of the scalar and tensor spectra that is nearly scale invariant over large scales, which is dictated by the first phase of SR in our model. Such primordial scalar and tensor power spectra are conventionally parameterized as

$$\mathcal{P}_s(k) = A_s \left(\frac{k}{k_*} \right)^{n_s - 1}, \quad (\text{A.1})$$

$$\mathcal{P}_T(k) = r \mathcal{P}_s(k_*). \quad (\text{A.2})$$

The parameters describing these power-law forms of spectra are well constrained to the following values: $\ln(10^{10} A_s) = 3.046 \pm 0.014$, $n_s = 0.9652 \pm 0.0041$ and $r < 0.019$ at the level of $1\text{-}\sigma$ from our analysis against CMB dataset (Planck2018+BK15) [123, 124]. We do not consider additional parameters such as running of the spectral index and the tilt of the tensor power in the above parametrization.

In a typical slow-roll inflationary model, we can show that the quantities describing the power-law forms above can be related to the parameters determining the background evolution of inflation using the slow-roll approximation, in the following way:

$$A_s \simeq \frac{H(k_*)}{8\pi^2 \epsilon_1(k_*)}, \quad (\text{A.3})$$

$$n_s \simeq 1 - 2\epsilon_1(k_*) - \epsilon_2(k_*), \quad (\text{A.4})$$

$$r \simeq 16\epsilon_1(k_*). \quad (\text{A.5})$$

The quantities H , ϵ_1 and ϵ_2 above are evaluated at the moment when the pivot scale k_* exits the Hubble radius [satisfying the condition $k_* = a(N)H(N)$] during inflation. These relations, although are true for a slow-roll model of inflation, are also valid for describing the power spectra in USR, but only for large scales that exit Hubble radius much before the onset of USR. This can be understood as the modes well into the super-Hubble regime during USR not experiencing much effect in their evolution due to USR dynamics.

Parameters	Minimum	Maximum
$\log_{10}(H_i)$	-5.40	-4.90
$\log_{10}(\epsilon_{1_i})$	-4.25	-3.40
$\log_{10}(\epsilon_{2_i})$	-2.50	-1.20

Table 2. The priors on the parameters that determine the spectra over large scales while comparing the model against dataset of CMB from `Planck 2018` and `BK15` are mentioned here. We have varied these in logarithmic scale to explore a wide region in the parameter space.

Thus one can argue that we may fix the initial values of H , ϵ_1 and ϵ_2 in USR model such that they lead to the best-fit values of A_s , n_s and r over large scales, while varying only the parameters of USR, namely N_1 and ΔN to inspect the effect over small scales when comparing against data. However, we should caution that time evolution of H , ϵ_1 and ϵ_2 are related to one another as

$$H(N) = H_i \exp \left[- \int_0^N dN \epsilon_1(N) \right], \quad (\text{A.6})$$

$$\epsilon_1(N) = \epsilon_{1_i} \exp \left[\int_0^N dN \epsilon_2(N) \right]. \quad (\text{A.7})$$

So, the choice of the initial values for them are not completely independent as they have a non-trivial, albeit a mild, dependence on each other. Besides, comparing an inflationary model with five parameters against an extended dataset, while computing the scalar and tensor power spectra numerically at each point, increases the computational complexity of data analysis.

We adopted the following method to arrive at bounds on the parameters of interest. We compared the model of USR varying all the five relevant parameters against just the CMB likelihoods (`Planck 2018` and `BK15`). The priors on the standard cosmological parameters are set as given in Tab. 1, and the priors on parameters determining USR are set to be $N_1 = [25, 35]$ and $\Delta N = [0, 1]$ as in the main text. The priors on the three parameters H_i , ϵ_{1_i} and ϵ_{2_i} , that are varied additionally are set as given in Tab. A. We then perform an MCMC analysis, where we numerically compute the primordial scalar and tensor power spectra at each sampled point in the parameter space. On such a comparison against the CMB dataset, we arrived at the best-fit values for H_i , ϵ_{1_i} and ϵ_{2_i} , along with constraints on N_1 and ΔN . We then fixed these three parameters at their best-fit values to compare the model against further datasets as presented in the main text. We also verified that the constraints on N_1 and ΔN are not altered as we fix the three parameters while comparing against the same dataset.

The posterior distribution of the five parameters describing the USR model is presented in Fig. 8. The four cosmological parameters, $\Omega_c h^2$, $\Omega_b h^2$, θ_{MC} and τ are evidently constrained around same values with same levels of variances around their mean, in both PL and our model. This confirms that the seemingly stronger bounds on them, seen earlier in Figs. 3 and 4 are essentially due to fixing of the values of H_i , ϵ_{1_i} and ϵ_{2_i} , and are not to be considered any improvement in their estimates.

As to the inflationary parameters of our model, we can understand the contours by the corresponding behaviours of A_s , n_s and r they lead to. The contours of H_i and ϵ_{1_i} are tightly correlated as expected. This is because $A_s \propto H^2(k_*)/\epsilon_1(k_*)$ and so $H_i \propto \epsilon_{1_i}$. The parameter

ϵ_{1i} is relatively unconstrained since it mainly determines r which only has an upper bound of $r < 10^{-2}$. On the other hand, ϵ_{2i} is constrained as $-1.52 < \log_{10}(\epsilon_{2i}) < -1.42$ at the level of $1-\sigma$, as it is responsible for achieving appropriate value of $n_s \sim 1 - \epsilon_{2i}$ and n_s is tightly constrained. Based on these results we fix $H_i = 7.3 \times 10^{-6} M_{\text{Pl}}$, $\epsilon_{1i} = 1.5 \times 10^{-4}$ and $\epsilon_{2i} = 3.5 \times 10^{-2}$ in our analyses presented in the main text. These choices lead to corresponding values of $A_s = 2.12 \times 10^{-9}$, $n_s = 0.96$ and $r = 5.04 \times 10^{-3}$ over large scales.

Note that contours on N_1 and ΔN broadly have the same shape and bounds as in Fig. 3. This informs us of the independence of the dynamics of USR and SR in our model. Since we are mainly interested in arriving at bounds on N_1 (or equivalently \bar{N}_1) and ΔN , this exercise justifies fixing the H_i , ϵ_{1i} and ϵ_{2i} at the values that have been used in our analyses in the main text.

We should add that there may be certain potentials realizing a phase of USR during inflation, where the parameters dictating USR dynamics may also play a role in the shape of spectra over large scales. There may arise a strong running of the scalar spectral index when USR is achieved with some smooth forms of potentials. These effects can alter fit to CMB and hence can push the onset of USR further to a later time during inflation. Thus, our bounds on \bar{N}_1 are relatively conservative in providing the earliest possible onset of USR.

References

- [1] O. Özsoy and G. Tasinato, *Inflation and Primordial Black Holes*, *Universe* **9** (2023), no. 5 203, [[arXiv:2301.03600](#)].
- [2] G. Domènech, *Scalar Induced Gravitational Waves Review*, *Universe* **7** (2021), no. 11 398, [[arXiv:2109.01398](#)].
- [3] **LISA Cosmology Working Group** Collaboration, E. Bagui et al., *Primordial black holes and their gravitational-wave signatures*, [arXiv:2310.19857](#).
- [4] **LIGO Scientific, Virgo** Collaboration, B. P. Abbott et al., *GWTC-1: A Gravitational-Wave Transient Catalog of Compact Binary Mergers Observed by LIGO and Virgo during the First and Second Observing Runs*, *Phys. Rev. X* **9** (2019), no. 3 031040, [[arXiv:1811.12907](#)].
- [5] **LIGO Scientific, VIRGO** Collaboration, R. Abbott et al., *GWTC-2.1: Deep Extended Catalog of Compact Binary Coalescences Observed by LIGO and Virgo During the First Half of the Third Observing Run*, [arXiv:2108.01045](#).
- [6] **LIGO Scientific, VIRGO, KAGRA** Collaboration, R. Abbott et al., *GWTC-3: Compact Binary Coalescences Observed by LIGO and Virgo During the Second Part of the Third Observing Run*, [arXiv:2111.03606](#).
- [7] **NANOGrav** Collaboration, G. Agazie et al., *The NANOGrav 15 yr Data Set: Evidence for a Gravitational-wave Background*, *Astrophys. J. Lett.* **951** (2023), no. 1 L8, [[arXiv:2306.16213](#)].
- [8] **EPTA, InPTA:** Collaboration, J. Antoniadis et al., *The second data release from the European Pulsar Timing Array - III. Search for gravitational wave signals*, *Astron. Astrophys.* **678** (2023) A50, [[arXiv:2306.16214](#)].
- [9] S. Bird, I. Cholis, J. B. Muñoz, Y. Ali-Haïmoud, M. Kamionkowski, E. D. Kovetz, A. Raccanelli, and A. G. Riess, *Did LIGO detect dark matter?*, *Phys. Rev. Lett.* **116** (2016), no. 20 201301, [[arXiv:1603.00464](#)].
- [10] M. Sasaki, T. Suyama, T. Tanaka, and S. Yokoyama, *Primordial Black Hole Scenario for the Gravitational-Wave Event GW150914*, *Phys. Rev. Lett.* **117** (2016), no. 6 061101, [[arXiv:1603.08338](#)]. [erratum: *Phys. Rev. Lett.*121,no.5,059901(2018)].

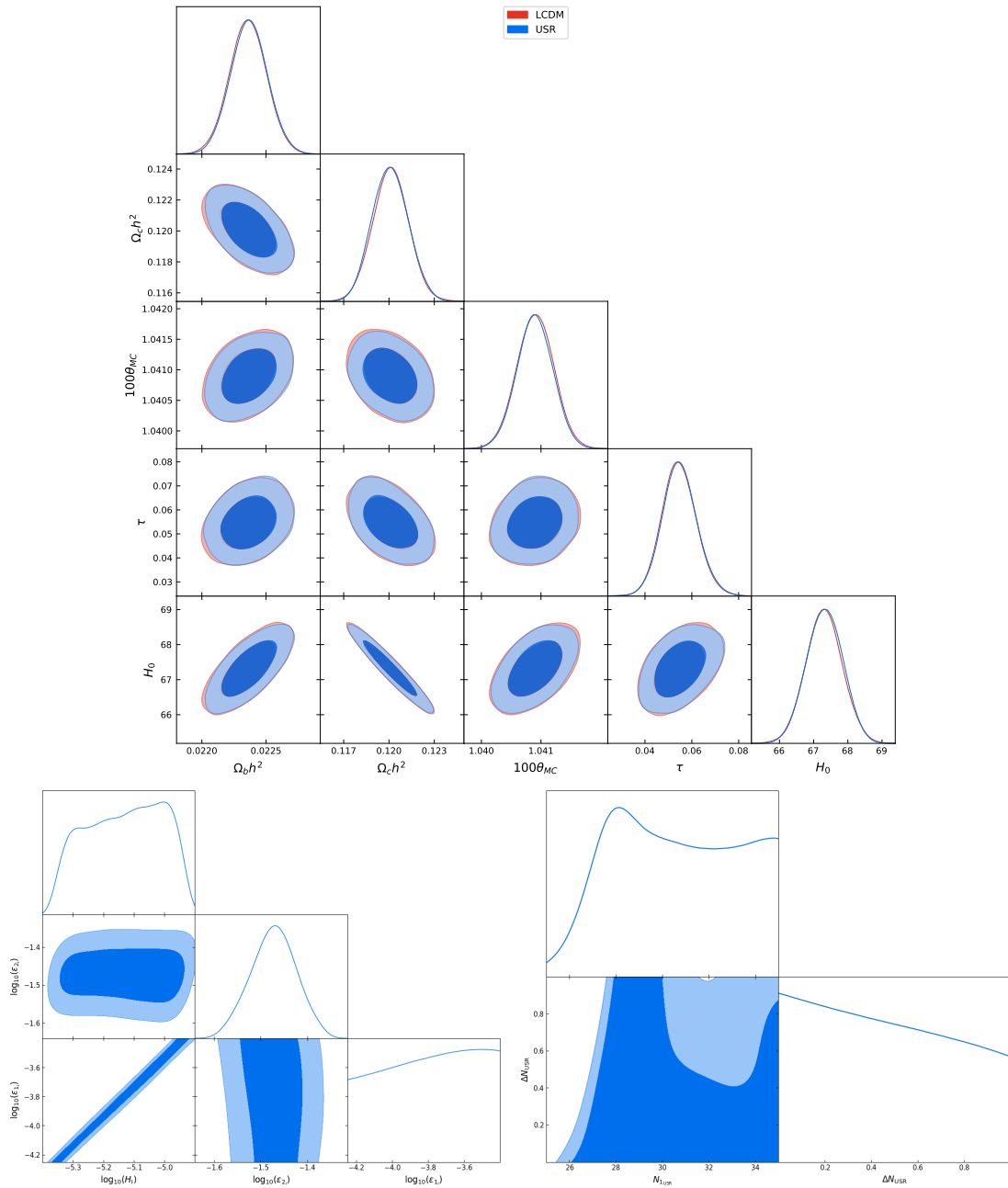


Figure 8. The $1\text{-}\sigma$ and $2\text{-}\sigma$ contours of the posterior distribution of parameters for the case when the five parameters of USR model are varied when comparing against CMB (Planck2018+BK15) are presented here. The standard cosmological parameters are presented on the top panel. Note that their distributions are the essentially the same between PL and USR models. The three parameters that determine the spectrum on large scales, $\log_{10}(H_i)$, $\log_{10}(\epsilon_{1i})$ and $\log_{10}(\epsilon_{2i})$, are presented (on bottom left) along with the parameters dictating USR epoch, N_1 and ΔN (on bottom right). Note that the constraints on N_1 and ΔN are similar to that in Fig. 3, where we have compared against the same dataset, but with fixed values for the other three parameters.

- [11] V. De Luca, G. Franciolini, P. Pani, and A. Riotto, *Primordial Black Holes Confront LIGO/Virgo data: Current situation*, *JCAP* **06** (2020) 044, [[arXiv:2005.05641](https://arxiv.org/abs/2005.05641)].

- [12] K. Jedamzik, *Primordial Black Hole Dark Matter and the LIGO/Virgo observations*, *JCAP* **09** (2020) 022, [[arXiv:2006.11172](#)].
- [13] K. Jedamzik, *Consistency of Primordial Black Hole Dark Matter with LIGO/Virgo Merger Rates*, *Phys. Rev. Lett.* **126** (2021), no. 5 051302, [[arXiv:2007.03565](#)].
- [14] Z.-C. Chen and A. Hall, *Confronting primordial black holes with LIGO-Virgo-KAGRA and the Einstein Telescope*, [arXiv:2402.03934](#).
- [15] **NANOGrav** Collaboration, A. Afzal et al., *The NANOGrav 15 yr Data Set: Search for Signals from New Physics*, *Astrophys. J. Lett.* **951** (2023), no. 1 L11, [[arXiv:2306.16219](#)].
- [16] Y.-F. Cai, X.-C. He, X.-H. Ma, S.-F. Yan, and G.-W. Yuan, *Limits on scalar-induced gravitational waves from the stochastic background by pulsar timing array observations*, *Sci. Bull.* **68** (2023) 2929–2935, [[arXiv:2306.17822](#)].
- [17] S. Vagnozzi, *Inflationary interpretation of the stochastic gravitational wave background signal detected by pulsar timing array experiments*, *JHEAp* **39** (2023) 81–98, [[arXiv:2306.16912](#)].
- [18] S. Choudhury, *Single field inflation in the light of Pulsar Timing Array Data: Quintessential interpretation of blue tilted tensor spectrum through Non-Bunch Davies initial condition*, *Eur. Phys. J. C* **84** (2024) 278, [[arXiv:2307.03249](#)].
- [19] H. Firouzjahi and A. Talebian, *Induced gravitational waves from ultra slow-roll inflation and pulsar timing arrays observations*, *JCAP* **10** (2023) 032, [[arXiv:2307.03164](#)].
- [20] B. Das, N. Jaman, and M. Sami, *Gravitational wave background from quintessential inflation and NANOGrav data*, *Phys. Rev. D* **108** (2023), no. 10 103510, [[arXiv:2307.12913](#)].
- [21] J. Ellis, M. Fairbairn, G. Franciolini, G. Hütsi, A. Iovino, M. Lewicki, M. Raidal, J. Urrutia, V. Vaskonen, and H. Veermäe, *What is the source of the PTA GW signal?*, *Phys. Rev. D* **109** (2024), no. 2 023522, [[arXiv:2308.08546](#)].
- [22] M. R. Gangopadhyay, V. V. Godithi, K. Ichiki, R. Intui, T. Kajino, A. Manusankar, G. J. Mathews, and Yogesh, *Is the NANOGrav detection evidence of resonant particle creation during inflation?*, [arXiv:2309.03101](#).
- [23] Q. Fei, *Constraints on the primordial curvature power spectrum by pulsar timing array data: a polynomial parameterization approach*, *Commun. Theor. Phys.* **76** (2024), no. 1 015404, [[arXiv:2310.17199](#)].
- [24] S. Choudhury, A. Karde, S. Panda, and M. Sami, *Realisation of the ultra-slow roll phase in Galileon inflation and PBH overproduction*, [arXiv:2401.10925](#).
- [25] A. A. Starobinsky, *Spectrum of adiabatic perturbations in the universe when there are singularities in the inflation potential*, *JETP Lett.* **55** (1992) 489–494.
- [26] D. K. Hazra, M. Aich, R. K. Jain, L. Sriramkumar, and T. Souradeep, *Primordial features due to a step in the inflaton potential*, *JCAP* **10** (2010) 008, [[arXiv:1005.2175](#)].
- [27] J. Martin, L. Sriramkumar, and D. K. Hazra, *Sharp inflaton potentials and bi-spectra: Effects of smoothening the discontinuity*, *JCAP* **09** (2014) 039, [[arXiv:1404.6093](#)].
- [28] J. Garcia-Bellido and E. Ruiz Morales, *Primordial black holes from single field models of inflation*, *Phys. Dark Univ.* **18** (2017) 47–54, [[arXiv:1702.03901](#)].
- [29] C. Germani and T. Prokopec, *On primordial black holes from an inflection point*, *Phys. Dark Univ.* **18** (2017) 6–10, [[arXiv:1706.04226](#)].
- [30] G. Ballesteros and M. Taoso, *Primordial black hole dark matter from single field inflation*, *Phys. Rev. D* **97** (2018), no. 2 023501, [[arXiv:1709.05565](#)].
- [31] J. M. Ezquiaga, J. Garcia-Bellido, and E. Ruiz Morales, *Primordial Black Hole production in Critical Higgs Inflation*, *Phys. Lett.* **B776** (2018) 345–349, [[arXiv:1705.04861](#)].

- [32] F. Bezrukov, M. Pauly, and J. Rubio, *On the robustness of the primordial power spectrum in renormalized Higgs inflation*, *JCAP* **02** (2018) 040, [[arXiv:1706.05007](#)].
- [33] M. Drees and Y. Xu, *Overshooting, Critical Higgs Inflation and Second Order Gravitational Wave Signatures*, *Eur. Phys. J. C* **81** (2021), no. 2 182, [[arXiv:1905.13581](#)].
- [34] V. Atal, J. Garriga, and A. Marcos-Caballero, *Primordial black hole formation with non-Gaussian curvature perturbations*, *JCAP* **09** (2019) 073, [[arXiv:1905.13202](#)].
- [35] S. S. Mishra and V. Sahni, *Primordial Black Holes from a tiny bump/dip in the Inflaton potential*, *JCAP* **04** (2020) 007, [[arXiv:1911.00057](#)].
- [36] G. Ballesteros, J. Rey, M. Taoso, and A. Urbano, *Primordial black holes as dark matter and gravitational waves from single-field polynomial inflation*, [[arXiv:2001.08220](#)].
- [37] K. Kefala, G. P. Kodaxis, I. D. Stamou, and N. Tetradis, *Features of the inflaton potential and the power spectrum of cosmological perturbations*, *Phys. Rev. D* **104** (2021), no. 2 023506, [[arXiv:2010.12483](#)].
- [38] M. Braglia, D. K. Hazra, F. Finelli, G. F. Smoot, L. Sriramkumar, and A. A. Starobinsky, *Generating PBHs and small-scale GWs in two-field models of inflation*, *JCAP* **08** (2020) 001, [[arXiv:2005.02895](#)].
- [39] R. Zheng and T. Q. Shi, Jiaming and, *On primordial black holes and secondary gravitational waves generated from inflation with solo/multi-bumpy potential **, *Chin. Phys. C* **46** (2022), no. 4 045103, [[arXiv:2106.04303](#)].
- [40] M. Braglia, A. Linde, R. Kallosh, and F. Finelli, *Hybrid α -attractors, primordial black holes and gravitational wave backgrounds*, *JCAP* **04** (2023) 033, [[arXiv:2211.14262](#)].
- [41] H.-R. Zhao, Y.-C. Liu, J.-X. Zhao, and N. Li, *The evolution of the primordial curvature perturbation in the ultraslow-roll inflation*, *Eur. Phys. J. C* **83** (2023), no. 9 783.
- [42] H. V. Ragavendra and L. Sriramkumar, *Observational Imprints of Enhanced Scalar Power on Small Scales in Ultra Slow Roll Inflation and Associated Non-Gaussianities*, *Galaxies* **11** (2023), no. 1 34, [[arXiv:2301.08887](#)].
- [43] C. T. Byrnes, P. S. Cole, and S. P. Patil, *Steepest growth of the power spectrum and primordial black holes*, *JCAP* **06** (2019) 028, [[arXiv:1811.11158](#)].
- [44] H. Motohashi, S. Mukohyama, and M. Oliosi, *Constant Roll and Primordial Black Holes*, *JCAP* **03** (2020) 002, [[arXiv:1910.13235](#)].
- [45] G. Tasinato, *An analytic approach to non-slow-roll inflation*, *Phys. Rev. D* **103** (2021), no. 2 023535, [[arXiv:2012.02518](#)].
- [46] H. V. Ragavendra, P. Saha, L. Sriramkumar, and J. Silk, *Primordial black holes and secondary gravitational waves from ultraslow roll and punctuated inflation*, *Phys. Rev. D* **103** (2021), no. 8 083510, [[arXiv:2008.12202](#)].
- [47] G. Franciolini and A. Urbano, *Primordial black hole dark matter from inflation: The reverse engineering approach*, *Phys. Rev. D* **106** (2022), no. 12 123519, [[arXiv:2207.10056](#)].
- [48] O. Özsoy and G. Tasinato, *On the slope of the curvature power spectrum in non-attractor inflation*, *JCAP* **04** (2020) 048, [[arXiv:1912.01061](#)].
- [49] S. Balaji, H. V. Ragavendra, S. K. Sethi, J. Silk, and L. Sriramkumar, *Observing Nulling of Primordial Correlations via the 21-cm Signal*, *Phys. Rev. Lett.* **129** (2022), no. 26 261301, [[arXiv:2206.06386](#)].
- [50] K.-W. Ng and Y.-P. Wu, *Constant-rate inflation: primordial black holes from conformal weight transitions*, *JHEP* **11** (2021) 076, [[arXiv:2102.05620](#)].
- [51] P. S. Cole, A. D. Gow, C. T. Byrnes, and S. P. Patil, *Steepest growth re-examined:*

repercussions for primordial black hole formation, [arXiv:2204.07573](#).

- [52] N. Bhaumik and R. K. Jain, *Primordial black holes dark matter from inflection point models of inflation and the effects of reheating*, [arXiv:1907.04125](#). [JCAP2001,037(2020)].
- [53] L. Iacconi, H. Assadullahi, M. Fasiello, and D. Wands, *Revisiting small-scale fluctuations in α -attractor models of inflation*, *JCAP* **06** (2022), no. 06 007, [[arXiv:2112.05092](#)].
- [54] M. Cicoli, F. G. Pedro, and N. Pedron, *Secondary GWs and PBHs in string inflation: formation and detectability*, *JCAP* **08** (2022), no. 08 030, [[arXiv:2203.00021](#)].
- [55] A. Karam, N. Koivunen, E. Tomberg, V. Vaskonen, and H. Veermäe, *Anatomy of single-field inflationary models for primordial black holes*, *JCAP* **03** (2023) 013, [[arXiv:2205.13540](#)].
- [56] W. Qin, S. R. Geller, S. Balaji, E. McDonough, and D. I. Kaiser, *Planck constraints and gravitational wave forecasts for primordial black hole dark matter seeded by multifield inflation*, *Phys. Rev. D* **108** (2023), no. 4 043508, [[arXiv:2303.02168](#)].
- [57] M. Tagliacuzzi, M. Braglia, F. Finelli, and M. Pieroni, *The quest of CMB spectral distortions to probe the scalar-induced gravitational wave background interpretation in PTA data*, [arXiv:2310.08527](#).
- [58] J. C. Mather et al., *Measurement of the Cosmic Microwave Background spectrum by the COBE FIRAS instrument*, *Astrophys. J.* **420** (1994) 439–444.
- [59] D. J. Fixsen, E. S. Cheng, J. M. Gales, J. C. Mather, R. A. Shafer, and E. L. Wright, *The Cosmic Microwave Background spectrum from the full COBE FIRAS data set*, *Astrophys. J.* **473** (1996) 576, [[astro-ph/9605054](#)].
- [60] C.-A. Faucher-Giguere, J. X. Prochaska, A. Lidz, L. Hernquist, and M. Zaldarriaga, *A direct precision measurement of the intergalactic Ly α opacity at $2 \leq z \leq 4.2$* , *The Astrophysical Journal* **681** (2008), no. 2 831.
- [61] V. F. Mukhanov, H. A. Feldman, and R. H. Brandenberger, *Theory of cosmological perturbations. Part 1. Classical perturbations. Part 2. Quantum theory of perturbations. Part 3. Extensions*, *Phys. Rept.* **215** (1992) 203–333.
- [62] J. Martin, *Inflationary cosmological perturbations of quantum-mechanical origin*, *Lect. Notes Phys.* **669** (2005) 199–244, [[hep-th/0406011](#)].
- [63] W. H. Kinney, *TASI Lectures on Inflation*, [arXiv:0902.1529](#).
- [64] D. Baumann, *Inflation*, in *Physics of the large and the small, TASI 09, proceedings of the Theoretical Advanced Study Institute in Elementary Particle Physics, Boulder, Colorado, USA, 1-26 June 2009*, pp. 523–686, 2011. [arXiv:0907.5424](#).
- [65] L. Sriramkumar, *An introduction to inflation and cosmological perturbation theory*, [arXiv:0904.4584](#).
- [66] P. Carrilho, K. A. Malik, and D. J. Mulryne, *Dissecting the growth of the power spectrum for primordial black holes*, *Phys. Rev. D* **100** (2019), no. 10 103529, [[arXiv:1907.05237](#)].
- [67] O. Özsoy, S. Parameswaran, G. Tasinato, and I. Zavala, *Mechanisms for Primordial Black Hole Production in String Theory*, *JCAP* **1807** (2018) 005, [[arXiv:1803.07626](#)].
- [68] O. Özsoy and G. Tasinato, *Consistency conditions and primordial black holes in single field inflation*, *Phys. Rev. D* **105** (2022), no. 2 023524, [[arXiv:2111.02432](#)].
- [69] J. Liu, Z.-K. Guo, and R.-G. Cai, *Analytical approximation of the scalar spectrum in the ultraslow-roll inflationary models*, *Phys. Rev. D* **101** (2020), no. 8 083535, [[arXiv:2003.02075](#)].
- [70] R. K. Jain, P. Chingangbam, J.-O. Gong, L. Sriramkumar, and T. Souradeep, *Punctuated inflation and the low CMB multipoles*, *JCAP* **01** (2009) 009, [[arXiv:0809.3915](#)].

- [71] R. K. Jain, P. Chingangbam, L. Sriramkumar, and T. Souradeep, *The tensor-to-scalar ratio in punctuated inflation*, *Phys. Rev. D* **82** (2010) 023509, [[arXiv:0904.2518](#)].
- [72] M. H. Qureshi, A. Iqbal, M. A. Malik, and T. Souradeep, *Low- ℓ power suppression in punctuated inflation*, *JCAP* **04** (2017) 013, [[arXiv:1610.05776](#)].
- [73] H. V. Ragavendra, D. Chowdhury, and L. Sriramkumar, *Suppression of scalar power on large scales and associated bispectra*, *Phys. Rev. D* **106** (2022), no. 4 043535, [[arXiv:2003.01099](#)].
- [74] **Planck** Collaboration, N. Aghanim et al., *Planck 2018 results. V. CMB power spectra and likelihoods*, *Astron. Astrophys.* **641** (2020) A5, [[arXiv:1907.12875](#)].
- [75] BICEP2 Collaboration, Keck Array Collaboration, P. A. R. Ade, Z. Ahmed, R. W. Aikin, K. D. Alexander, D. Barkats, S. J. Benton, C. A. Bischoff, J. J. Bock, R. Bowens-Rubin, J. A. Brevik, I. Buder, E. Bullock, V. Buza, J. Connors, J. Cornelison, B. P. Crill, M. Crumrine, M. Dierickx, L. Duband, C. Dvorkin, J. P. Filippini, S. Fliescher, J. Grayson, G. Hall, M. Halpern, S. Harrison, S. R. Hildebrandt, G. C. Hilton, H. Hui, K. D. Irwin, J. Kang, K. S. Karkare, E. Karpel, J. P. Kaufman, B. G. Keating, S. Kefeli, S. A. Kernasovskiy, J. M. Kovac, C. L. Kuo, N. A. Larsen, K. Lau, E. M. Leitch, M. Lueker, K. G. Megerian, L. Moncelsi, T. Namikawa, C. B. Netterfield, H. T. Nguyen, R. O’Brient, R. W. Ogburn, S. Palladino, C. Pryke, B. Racine, S. Richter, A. Schillaci, R. Schwarz, C. D. Sheehy, A. Soliman, T. St. Germaine, Z. K. Staniszewski, B. Steinbach, R. V. Sudiwala, G. P. Teply, K. L. Thompson, J. E. Tolán, C. Tucker, A. D. Turner, C. Umiltà, A. G. Viereg, A. Wandui, A. C. Weber, D. V. Wiebe, J. Willmert, C. L. Wong, W. L. K. Wu, H. Yang, K. W. Yoon, and C. Zhang, *Constraints on Primordial Gravitational Waves Using Planck, WMAP, and New BICEP2/Keck Observations through the 2015 Season*, *Phys. Rev. Lett.* **121** (Nov., 2018) 221301, [[arXiv:1810.05216](#)].
- [76] **BOSS** Collaboration, S. Alam et al., *The clustering of galaxies in the completed SDSS-III Baryon Oscillation Spectroscopic Survey: cosmological analysis of the DR12 galaxy sample*, *Mon. Not. Roy. Astron. Soc.* **470** (2017), no. 3 2617–2652, [[arXiv:1607.03155](#)].
- [77] **Pan-STARRS1** Collaboration, D. M. Scolnic et al., *The Complete Light-curve Sample of Spectroscopically Confirmed SNe Ia from Pan-STARRS1 and Cosmological Constraints from the Combined Pantheon Sample*, *Astrophys. J.* **859** (2018), no. 2 101, [[arXiv:1710.00845](#)].
- [78] A. Drlica-Wagner, I. Sevilla-Noarbe, E. S. Rykoff, R. A. Gruendl, B. Yanny, D. L. Tucker, B. Hoyle, A. C. Rosell, G. M. Bernstein, K. Bechtol, M. R. Becker, A. Benoit-Lévy, E. Bertin, M. C. Kind, C. Davis, J. de Vicente, H. T. Diehl, D. Gruen, W. G. Hartley, B. Leistedt, T. S. Li, J. L. Marshall, E. Neilsen, M. M. Rau, E. Sheldon, J. Smith, M. A. Troxel, S. Wyatt, Y. Zhang, T. M. C. Abbott, F. B. Abdalla, S. Allam, M. Banerji, D. Brooks, E. Buckley-Geer, D. L. Burke, D. Capozzi, J. Carretero, C. E. Cunha, C. B. D’Andrea, L. N. da Costa, D. L. DePoy, S. Desai, J. P. Dietrich, P. Doel, A. E. Evrard, A. F. Neto, B. Flaugher, P. Fosalba, J. Frieman, J. García-Bellido, D. W. Gerdes, T. Giannantonio, J. Gschwend, G. Gutierrez, K. Honscheid, D. J. James, T. Jeltema, K. Kuehn, S. Kuhlmann, N. Kuropatkin, O. Lahav, M. Lima, H. Lin, M. A. G. Maia, P. Martini, R. G. McMahon, P. Melchior, F. Menanteau, R. Miquel, R. C. Nichol, R. L. C. Ogando, A. A. Plazas, A. K. Romer, A. Roodman, E. Sanchez, V. Scarpine, R. Schindler, M. Schubnell, M. Smith, R. C. Smith, M. Soares-Santos, F. Sobreira, E. Suchyta, G. Tarle, V. Vikram, A. R. Walker, R. H. Wechsler, J. Zuntz, and D. Collaboration), *Dark energy survey year 1 results: The photometric data set for cosmology*, *The Astrophysical Journal Supplement Series* **235** (apr, 2018) 33.
- [79] A. Lewis and S. Bridle, *Cosmological parameters from CMB and other data: A Monte Carlo approach*, *Phys. Rev. D* **66** (2002) 103511, [[astro-ph/0205436](#)].
- [80] A. Lewis, A. Challinor, and A. Lasenby, *Efficient computation of CMB anisotropies in closed FRW models*, *Astrophys. J.* **538** (2000) 473–476, [[astro-ph/9911177](#)].
- [81] A. Lewis, *GetDist: a Python package for analysing Monte Carlo samples*, [[arXiv:1910.13970](#)].

- [82] J. Chluba et al., *Spectral Distortions of the CMB as a Probe of Inflation, Recombination, Structure Formation and Particle Physics: Astro2020 Science White Paper*, *Bull. Am. Astron. Soc.* **51** (2019), no. 3 184, [[arXiv:1903.04218](#)].
- [83] S. Dodelson, *Modern Cosmology*. Academic Press, Elsevier Science, 2003.
- [84] R. Murgia, A. Merle, M. Viel, M. Totzauer, and A. Schneider, "Non-cold" dark matter at small scales: a general approach, *JCAP* **11** (2017) 046, [[arXiv:1704.07838](#)].
- [85] H. Bi and A. F. Davidsen, *Evolution of structure in the intergalactic medium and the nature of the Ly α forest*, *The Astrophysical Journal* **479** (1997), no. 2 523.
- [86] L. Hui and N. Y. Gnedin, *Equation of state of the photoionized intergalactic medium*, *Monthly Notices of the Royal Astronomical Society* **292** (1997), no. 1 27–42.
- [87] T. R. Choudhury, R. Srianand, and T. Padmanabhan, *Semianalytic approach to understanding the distribution of neutral hydrogen in the universe: comparison of simulations with observations*, *The Astrophysical Journal* **559** (2001), no. 1 29.
- [88] K. L. Pandey and S. K. Sethi, *Probing primordial magnetic fields using Ly α clouds*, *The Astrophysical Journal* **762** (2012), no. 1 15.
- [89] A. K. Sarkar, K. L. Pandey, and S. K. Sethi, *Using the redshift evolution of the Lyman- α effective opacity as a probe of dark matter models*, *Journal of Cosmology and Astroparticle Physics* **2021** (2021), no. 10 077.
- [90] S. Bird, H. V. Peiris, M. Viel, and L. Verde, *Minimally parametric power spectrum reconstruction from the Lyman α forest*, *MNRAS* **413** (May, 2011) 1717–1728, [[arXiv:1010.1519](#)].
- [91] T. Bringmann, P. Scott, and Y. Akrami, *Improved constraints on the primordial power spectrum at small scales from ultracompact minihalos*, *Phys. Rev. D* **85** (2012) 125027, [[arXiv:1110.2484](#)].
- [92] A. Kogut, D. J. Fixsen, D. T. Chuss, J. Dotson, E. Dwek, M. Halpern, G. F. Hinshaw, S. M. Meyer, S. H. Moseley, M. D. Seiffert, D. N. Spergel, and E. J. Wollack, *The Primordial Inflation Explorer (PIXIE): a nulling polarimeter for cosmic microwave background observations*, *JCAP* **2011** (July, 2011) 025, [[arXiv:1105.2044](#)].
- [93] R.-g. Cai, S. Pi, and M. Sasaki, *Gravitational Waves Induced by non-Gaussian Scalar Perturbations*, *Phys. Rev. Lett.* **122** (2019), no. 20 201101, [[arXiv:1810.11000](#)].
- [94] C. Unal, *Imprints of Primordial Non-Gaussianity on Gravitational Wave Spectrum*, *Phys. Rev. D* **99** (2019), no. 4 041301, [[arXiv:1811.09151](#)].
- [95] V. Atal and G. Domènech, *Probing non-Gaussianities with the high frequency tail of induced gravitational waves*, *JCAP* **06** (2021) 001, [[arXiv:2103.01056](#)]. [Erratum: *JCAP* 10, E01 (2023)].
- [96] P. Adshead, K. D. Lozanov, and Z. J. Weiner, *Non-Gaussianity and the induced gravitational wave background*, *JCAP* **10** (2021) 080, [[arXiv:2105.01659](#)].
- [97] F. Zhang, J. Lin, and Y. Lu, *Double-peaked inflation model: Scalar induced gravitational waves and primordial-black-hole suppression from primordial non-Gaussianity*, *Phys. Rev. D* **104** (2021), no. 6 063515, [[arXiv:2106.10792](#)]. [Erratum: *Phys.Rev.D* 104, 129902 (2021)].
- [98] H. V. Ragavendra, *Accounting for scalar non-Gaussianity in secondary gravitational waves*, *Phys. Rev. D* **105** (2022), no. 6 063533, [[arXiv:2108.04193](#)].
- [99] S. Garcia-Saenz, L. Pinol, S. Renaux-Petel, and D. Werth, *No-go theorem for scalar-trispectrum-induced gravitational waves*, *JCAP* **03** (2023) 057, [[arXiv:2207.14267](#)].
- [100] C. Chen, A. Ota, H.-Y. Zhu, and Y. Zhu, *Missing one-loop contributions in secondary gravitational waves*, [arXiv:2210.17176](#).

- [101] J.-P. Li, S. Wang, Z.-C. Zhao, and K. Kohri, *Primordial non-Gaussianity f_{NL} and anisotropies in scalar-induced gravitational waves*, *JCAP* **10** (2023) 056, [[arXiv:2305.19950](#)].
- [102] G. Franciolini, A. Iovino, Junior., V. Vaskonen, and H. Veermae, *Recent Gravitational Wave Observation by Pulsar Timing Arrays and Primordial Black Holes: The Importance of Non-Gaussianities*, *Phys. Rev. Lett.* **131** (2023), no. 20 201401, [[arXiv:2306.17149](#)].
- [103] L. Liu, Z.-C. Chen, and Q.-G. Huang, *Implications for the non-Gaussianity of curvature perturbation from pulsar timing arrays*, *Phys. Rev. D* **109** (2024), no. 6 L061301, [[arXiv:2307.01102](#)].
- [104] C. Yuan, D.-S. Meng, and Q.-G. Huang, *Full analysis of the scalar-induced gravitational waves for the curvature perturbation with local-type non-Gaussianities*, *JCAP* **12** (2023) 036, [[arXiv:2308.07155](#)].
- [105] J.-P. Li, S. Wang, Z.-C. Zhao, and K. Kohri, *Complete Analysis of Scalar-Induced Gravitational Waves and Primordial Non-Gaussianities f_{NL} and g_{NL}* , [arXiv:2309.07792](#).
- [106] Z. Chang, Y.-T. Kuang, D. Wu, J.-Z. Zhou, and Q.-H. Zhu, *New constraints on primordial non-Gaussianity from missing two-loop contributions of scalar induced gravitational waves*, *Phys. Rev. D* **109** (2024), no. 4 L041303, [[arXiv:2311.05102](#)].
- [107] R. Inui, S. Jaraba, S. Kuroyanagi, and S. Yokoyama, *Constraints on Non-Gaussian primordial curvature perturbation from the LIGO-Virgo-KAGRA third observing run*, [arXiv:2311.05423](#).
- [108] Z. Chang, Y.-T. Kuang, D. Wu, and J.-Z. Zhou, *Probing scalar induced gravitational waves with PTA and LISA: The Importance of third order correction*, [arXiv:2312.14409](#).
- [109] T. Papanikolaou, X.-C. He, X.-H. Ma, Y.-F. Cai, E. N. Saridakis, and M. Sasaki, *New probe of non-Gaussianities with primordial black hole induced gravitational waves*, [arXiv:2403.00660](#).
- [110] C. T. Donnan, D. J. McLeod, J. S. Dunlop, R. J. McLure, A. C. Carnall, R. Begley, F. Cullen, M. L. Hamadouche, R. A. A. Bowler, D. Magee, H. J. McCracken, B. Milvang-Jensen, A. Moneti, and T. Targett, *The evolution of the galaxy UV luminosity function at redshifts $z \simeq 8 - 15$ from deep JWST and ground-based near-infrared imaging*, *Monthly Notices of the Royal Astronomical Society* **518** (Feb., 2023) 6011–6040, [[arXiv:2207.12356](#)].
- [111] I. Labbé, P. van Dokkum, E. Nelson, R. Bezanson, K. A. Suess, J. Leja, G. Brammer, K. Whitaker, E. Mathews, M. Stefanon, and B. Wang, *A population of red candidate massive galaxies 600 Myr after the Big Bang*, *Nature* **616** (Apr., 2023) 266–269, [[arXiv:2207.12446](#)].
- [112] W.-C. Syu, D.-S. Lee, and K.-W. Ng, *Quantum loop effects to the power spectrum of primordial perturbations during ultra slow-roll inflation*, *Phys. Rev. D* **101** (2020), no. 2 025013, [[arXiv:1907.13089](#)].
- [113] J. Kristiano and J. Yokoyama, *Ruling Out Primordial Black Hole Formation From Single-Field Inflation*, [arXiv:2211.03395](#).
- [114] K. Inomata, M. Braglia, X. Chen, and S. Renaux-Petel, *Questions on calculation of primordial power spectrum with large spikes: the resonance model case*, *JCAP* **04** (2023) 011, [[arXiv:2211.02586](#)]. [Erratum: *JCAP* 09, E01 (2023)].
- [115] S. Choudhury, M. R. Gangopadhyay, and M. Sami, *No-go for the formation of heavy mass Primordial Black Holes in Single Field Inflation*, [arXiv:2301.10000](#).
- [116] H. Firouzjahi, *Revisiting Loop Corrections in Single Field USR Inflation*, [arXiv:2311.04080](#).
- [117] S.-L. Cheng, D.-S. Lee, and K.-W. Ng, *Primordial perturbations from ultra-slow-roll single-field inflation with quantum loop effects*, [arXiv:2305.16810](#).
- [118] S. Maity, H. V. Ragavendra, S. K. Sethi, and L. Sriramkumar, *Loop contributions to the scalar power spectrum due to quartic order action in ultra slow roll inflation*, [arXiv:2307.13636](#).
- [119] A. Riotto, *The Primordial Black Hole Formation from Single-Field Inflation is Not Ruled*

Out, [arXiv:2301.00599](#).

- [120] H. Firouzjahi and A. Riotto, *Primordial Black Holes and Loops in Single-Field Inflation*, [arXiv:2304.07801](#).
- [121] J. Fumagalli, *Absence of one-loop effects on large scales from small scales in non-slow-roll dynamics*, [arXiv:2305.19263](#).
- [122] S.-L. Cheng, D.-S. Lee, and K.-W. Ng, *Power spectrum of primordial perturbations during ultra-slow-roll inflation with back reaction effects*, *Phys. Lett. B* **827** (2022) 136956, [[arXiv:2106.09275](#)].
- [123] **Planck** Collaboration, Y. Akrami et al., *Planck 2018 results. X. Constraints on inflation*, *Astron. Astrophys.* **641** (2020) A10, [[arXiv:1807.06211](#)].
- [124] **BICEP, Keck** Collaboration, P. A. R. Ade et al., *Improved Constraints on Primordial Gravitational Waves using Planck, WMAP, and BICEP/Keck Observations through the 2018 Observing Season*, *Phys. Rev. Lett.* **127** (2021), no. 15 151301, [[arXiv:2110.00483](#)].